Comprehensive Framework for Controlling Nonlinear Multispecies Water Quality Dynamics

Salma M. Elsherif, S.M.ASCE[1]; Ahmad F. Taha[2]; Ahmed A. Abokifa, A.M.ASCE[3]; and Lina Sela, A.M.ASCE[4]

Abstract: Tracing disinfectant (e.g., chlorine) and contaminants evolution in water networks requires the solution of one-dimensional (1D) advection-reaction (AR) partial differential equations (PDEs). With the absence of analytical solutions in many scenarios, numerical solutions require high-resolution time and space discretizations, resulting in large model dimensions. This adds complexity to the water quality control problem. In addition, considering multispecies water quality dynamics rather than the single-species dynamics produces a more accurate description of the reaction dynamics under abnormal hazardous conditions (e.g., contamination events). Yet, these dynamics introduce a nonlinear reaction formulation to the model. To that end, solving nonlinear 1D AR PDEs in real time is critical to achieving monitoring and control goals for various scaled networks with a high computational burden. In this work, we propose a novel comprehensive framework to overcome the large-dimensionality issue by introducing different approaches for applying model order reduction (MOR) algorithms to the nonlinear system followed by applying a real-time water quality regulation algorithm that is based on an advanced model to maintain desirable disinfectant levels in water networks under multispecies dynamics. The performance of this framework is validated using rigorous numerical case studies under a wide range of scenarios demonstrating the challenges associated with regulating water quality under such conditions. **DOI: 10.1061/JWRMD5.WRENG-6179.** © *2023 American Society of Civil Engineers.*

Introduction

Water quality (WQ) dynamics are widely modeled by one-dimensional (1D) advection-reaction (AR) partial differential equations (PDEs). These AR PDEs allow the tracing of the disinfectant and other chemical substances' evolution throughout the components of water distribution networks (WDNs). In most cases, analytical solutions are nonexistent to solve these PDEs network-wide. Nonetheless, PDEs can be solved using numerical techniques, although they require high-resolution time and space discretization. This results in high-dimension models that add computational burden to the problem of regulating water quality in drinking networks. That leads to physically driven models that are intractable when considering constrained control and WQ regulation algorithms.

Moreover, in water quality simulations, the most widely used decay and reaction model is the single-species model. In this model, disinfectant (i.e., chlorine) is assumed to decay at a constant rate that only accounts for purified water contamination levels. Yet, contamination sources can be from microbial or nonmicrobial components in the bulk flow, attached to the pipe walls, or contamination events that get intruded into the system (Palansooriya et al. 2020). This drives the need for a more accurate representation of these scenarios, which can be achieved by multispecies reaction dynamics. Multispecies dynamics enable the model to simulate chlorine evolution with the existence of another reactive component in the system. This representation duplicates the number of variables to be traced network-component-wide while unfortunately adding complexity to the model by introducing nonlinear reaction dynamics.

To that end, model order reduction (MOR) is an essential step to move forward in achieving a compact formulation of the multispecies water quality dynamics to be integrated into a model-based control framework. MOR techniques transform the full-order model (FOM) to a reduced-order model (ROM) in a way that preserves the structure, properties, and closed-form representation of the FOM while achieving the prespecified level of accuracy and reducing computational time. Eventually, the goal is to control chlorine injections dosed by rechlorination stations to maintain residual levels that meet water quality standards. That can be achieved by applying an effective control algorithm on the derived ROM.

Our group has been interested in various dimensions of this research area. A summary of our work and the prior literature is given next.

Literature Review

Hereinafter, we survey the literature on the topics of MOR for dynamic systems in general and water systems in particular and water quality regulation and control while highlighting the gaps and drawbacks motivating this paper's contributions.

MOR for Dynamic Systems

Several studies have proposed and implemented different MOR algorithms in various disciplines (e.g., electromagnetics, electromechanics, structural and fluid dynamics) where the large-dimensionality issue is faced (Moore 1981; Baur et al. 2014; Montier et al. 2017; Rutzmoser 2018). Most of these studies have applied either the singular value decomposition (SVD) approach (Rowley 2005; Willcox and Peraire 2002) or Krylov subspace

[1]Research Assistant, Dept. of Civil and Environmental Engineering, Vanderbilt Univ., Nashville, TN 37235; Faculty of Engineering, Dept. of Irrigation and Hydraulics Engineering, Cairo Univ., Giza 3725121, Egypt (corresponding author). ORCID: https://orcid.org/0000-0002-1814-9431. Email: salma.m.elsherif@vanderbilt.edu

[2]Dept. of Civil and Environmental Engineering, Vanderbilt Univ., Nashville, TN 37235. Email: ahmad.taha@vanderbilt.edu

[3]Assistant Professor, Dept. of Civil, Materials, and Environmental Engineering, Univ. of Illinois at Chicago, Chicago, IL 60607. ORCID: https://orcid.org/0000-0002-2474-6670. Email: abokifa@uic.edu

[4]Associate Professor, Dept. of Civil, Architecture, and Environmental Engineering, Univ. of Texas at Austin, Austin, TX 78712. ORCID: https://orcid.org/0000-0002-5834-8451. Email: linasela@utexas.edu

Note. This manuscript was submitted on March 10, 2023; approved on August 6, 2023; published online on November 20, 2023. Discussion period open until April 20, 2024; separate discussions must be submitted for individual papers. This paper is part of the ***Journal of Water Resources Planning and Management***, © ASCE, ISSN 0733-9496.

methods (Grimme 1997; Beattie and Gugercin 2008). Combining SVD and Krylov methods has been investigated and implemented in Gugercin (2008). In infrastructure networks, preserving the system's properties including stability, controllability, and observability is a major concern when applying MOR with the aim of applying a postreduction control. Nevertheless, Krylov methods do not preserve such properties, which limits their suitability to be used in our study (Baur et al. 2014).

Several SVD-based model reduction methods have been proposed for linear systems and more realizations and extensions have been investigated and integrated to tackle the reduction of nonlinear systems; a review of linear and nonlinear models order reduction can be found in Antoulas et al. (2000) and Kumar and Ezhilarasi (2022). The balanced truncation (BT) method (Moore 1981) is built based on both the controllability and observability Gramians for stable, linear systems. The study by Lall et al. (2002) extended BT to be applied to nonlinear systems, while Barrachina et al. (2005) and Zhou et al. (1999) built extensions for unstable systems. However, BT becomes computationally intractable for large-scale systems. Nevertheless, the famous widely used proper orthogonal decomposition (POD) method in fluid dynamics community (Sirovich 1987) is considered tractable at the expense of accuracy compared with BT. Yet, in some cases, where relatively lower accuracy is acceptable, POD may result in an unstable system even near stable equilibrium points depending on the actual formulation of the full-order model. Therefore, methods that balance between the BT and POD methods have been proposed to integrate the advantages of both methods into one. For example, Willcox and Peraire (2002) proposed a balanced method, but it failed to successfully reduce models when the number of outputs of the system is large. Conversely, the balanced POD (BPOD) (Rowley 2005) is tractable with an overall computation time similar to POD, but it computes adjoint snapshots to combine and balance controllability and observability similarly to BT, which is not raised in POD. Furthermore, POD can be extended to reduce the order of nonlinear systems by approximately projecting the nonlinearity term in the system to a subspace of the dynamics (Nguyen et al. 2020; Baur et al. 2014). Therefore, the nonlinear term is evaluated separately and approximated at only a small set of interpolation points (hyperparameter) using a combination of projection and interpolation methods such as the discrete empirical interpolation method (DEIM) (Nguyen et al. 2020), the gappy POD method (Galbally et al. 2010; Akkari et al. 2019), and the Gauss-Newton with approximated tensors (GNAT) method (Carlberg et al. 2013); refer to the review paper by Benner et al. (2015) for details.

MOR for Water Systems

Water systems model order reduction has been broadly investigated for network hydraulics over the past decades with a limited number of studies looking into MOR for water quality dynamics. These studies adopt different approaches to reduce the hydraulic model dimension by applying methods varying between performing nodal Gaussian elimination (Ulanicki et al. 1996), Gaussian elimination on the linearized form of the model and recovering the nonlinearity of the system as a postreduction step (Martnez Alzamora et al. 2014), genetic algorithm (Shamir and Salomons 2008), and system aggregation (Preis et al. 2011). Perelman and Ostfeld (2008) considered a coupled model that combines both hydraulics and water quality dynamics of the network and applied systems aggregation.

Recently, two studies have applied different approaches to cover the MOR for water quality dynamics. Elkhashap and Abel (2022) proposed reducing the order of the water quality model by formulating a bilinear spatially discretized but temporally continuous representation of the dynamics. This formulation augments the input vectors in a way that preserves the system's stability. The induced error between the actual and reduced-order models is minimized by the reduction of the $\mathcal{H}_2$-norm. In that study, water dynamics transport and reaction are simulated using advection-diffusion-reaction partial differential equations, which incorporate the diffusion term, In contrast, our work in this paper neglects the diffusion term's effect. Nonetheless, studies (Li et al. 2005; Shang et al. 2021) state that diffusion is dominant in network branches with significantly low velocities. To that end, it is an acceptable assumption to neglect the diffusion effect in networks with limited dead-end branches, higher velocities, and changing demands. On the other hand, augmenting and transferring the model into nonlinear formulation results in a more complex model when considering the multispecies nonlinear water quality dynamics and does not preserve the stability of the system.

Second, Wang et al. (2022) applies different SVD-based projection algorithms to reach a reduced-order water quality model including BT, POD, and BPOD in addition to preserving the stability of the BPOD method. Results have proven that the BPOD method is more usable while being computationally tractable and robust for zero and nonzero initial conditions. However, their model only includes single-species linear reaction dynamics where chlorine is assumed to be decaying at a constant rate, resulting in a linear state-space formulation. Therefore, this work allows filling the gap in applying MOR for multispecies nonlinear dynamics. Moreover, in their model, the explicit central Lax-Wendroff discretization scheme is used. However, the upwind schemes give a more accurate physical description of the advection-reaction problem. In our study, we apply the explicit and implicit upwind discretization schemes while highlighting the differences and the level of difficulty. Contrary to Fu et al. (2020), Lassila et al. (2014), and He and Durlofsky (2014), where MOR is performed for compositional simulation, Wang et al. (2022) state that it is considered as a prestep to apply an efficient control algorithm, which also applies to the work in this paper.

Water Quality Control

The topic of controlling chlorine has been covered in several studies with various algorithms, objectives, and constraints (Ohar and Ostfeld 2014; Ostfeld and Salomons 2006; Munavalli and Kumar 2003). Objectives vary between minimizing the cost of injecting chlorine into the system, maintaining minimal deviations from chlorine setpoint concentrations, minimizing the formation of the excess disinfection by-products (DBPs), and minimizing computational time (Fisher et al. 2018). The problem formulation is either a single-objective optimization problem or a multiobjective one with more of the aforementioned objectives. However, such studies do not build a closed-form representation of all inputs, states, and outputs that updates every specified time step over the simulation period and allows network-wide control. Wang et al. (2021, 2022) applied model predictive control (MPC) on the full-order and reduced-order single-species models in both studies with no clear explanation or extension for scenarios where multispecies dynamics take place.

Our Prior Work

We have been focusing on tackling and covering water quality modeling and control in WDNs. First, the problem of modeling and controlling single-species water quality dynamics is thoroughly investigated in Wang et al. (2021), followed by reducing this model's order and verifying the validity of controlling the reduced-order model in Wang et al. (2022). Moreover, as a first state-of-the-art attempt, Wang et al. (2023) identified single-species water quality models using only input-output experimental data and, accordingly, data-driven system identification algorithms. Last, a survey study on how to accurately simulate multispecies water quality dynamics

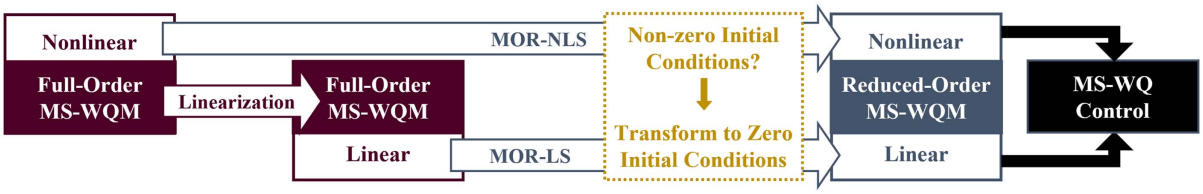

Fig. 1. Conceptual framework of the paper.

was conducted by Elsherif et al. (2022). This study built a closed-form, network– and control–theoretic representation of all system inputs, variables, and output measurements under such dynamics that give a more realistic WQ formulation. The performance of this formulation was validated using the widely used simulation tool EPANET and its multispecies water quality simulation extension, EPANET-MSX (Rossman et al. 2020). However, controlling chlorine under multispecies dynamics, based on a control–theoretic explicit model, to the authors' knowledge, has not been investigated—a gap that is filled in this paper.

Paper Contributions

This paper's major objective is to investigate the implementation and complexity of regulating and controlling chlorine levels under multispecies water quality. The detailed paper contributions are as follows:

- Construct and propose a comprehensive framework to overcome the large-dimensionality issue associated with discretizing 1D AR PDEs and the complexity associated with the nonlinearity of the multispecies water quality dynamics. Different paths can be taken, starting by linearizing the system and applying MOR for linear systems (MOR-LS). Another path is to consider the nonlinear MOR (MOR-NLS) algorithm on the original FOM.
- Utilize the reduced-order models in an MPC algorithm and compare them with each other and with the original FOMs. Also, we compare the results of the MPC algorithm when applied to both single-species and multispecies dynamics, illustrating the challenges involved in controlling chlorine levels within the context of multispecies water quality dynamics.
- Position the framework in a generalized scalable form in the sense that simplifications are included to consider single-species water dynamics, and differentiations are suggested to consider chlorine linear and nonlinear decay and reaction models that have been developed in the literature to simulate various events and scenarios.
- Validate the performance of the framework using thorough numerical case studies to test accuracy, computational burden, and robustness to the system hydraulics changes.

Our proposed framework is illustrated in Fig. 1. As shown, different approaches can be followed to formulate a reduced-order model to be controlled for the multispecies water quality model. Each step to be taken and each path to be chosen is explained in the following sections of the paper. The paper's sections are organized as follows: "State-Space Multispecies Water Quality Model" provides the formulation of the state-space representation of the multispecies water quality model (MS-WQM). This formulation is based on the transport and reaction model in pipes, mass balance for the other network components, and the multispecies dynamics expression. "Model Order Reduction and Transformation of MS-WQM" provides full descriptions of the methods used in our framework to reach a compact reduced-order model. "Real-Time Regulation of MS-WQM via Model Predictive Control and McCormick Relaxations" introduces the control problem and its implementation on the linear and nonlinear ROM. "Case Studies" showcases the framework performance on different networks under a wide range of scenarios. "Conclusion, Paper's Limitations, and Recommendations for Future Work" comes last.

State-Space Multispecies Water Quality Model

We model the WDN by a directed graph $\mathcal{G} = (N, \mathcal{L})$. The set $\mathcal{N}$ defines the nodes and is partitioned as $\mathcal{N} = \mathcal{J} \cup \mathcal{T} \cup \mathcal{R}$ where sets $\mathcal{J}$, $\mathcal{T}$, and $\mathcal{R}$ are collections of junctions, tanks, and reservoirs. Let $\mathcal{L} \subseteq \mathcal{N} \times \mathcal{N}$ be the set of links, and defines the partition, $\mathcal{L} = \mathcal{P} \cup \mathcal{M} \times \mathcal{V}$ where sets, $\mathcal{P}$, $\mathcal{M}$, and $\mathcal{V}$ represent the collection of pipes, pumps, and valves. The total number of states is $n_x = n_L + n_N$, where n_L and n_N are numbers of links and nodes. The number of reservoirs, junctions, tanks, pumps, valves, and pipes are $n_\mathrm{R}, n_\mathrm{J}, n_\mathrm{TK}, n_\mathrm{M}, n_\mathrm{V}$, and n_P. Each pipe i with length L_i is spatially discretized and split into s_{L_i} segments. Hence, the number of links is expressed as $n_\mathrm{L} = n_\mathrm{M} + n_\mathrm{V} + \sum_{i=1}^{n_\mathrm{P}} s_{L_i}$, while $n_\mathrm{N} = n_\mathrm{R} + n_\mathrm{J} + n_\mathrm{TK}$ is the number of nodes.

In this paper, the state-space representation is formulated for multispecies dynamics with two chemicals: chlorine and a fictitious reactant. The system representation of the two species, which is able to capture chemicals evolution, booster stations injections, and sensors measurements, is expressed by a nonlinear difference equation (NDE) as follows:

$$\underbrace{\begin{bmatrix} \boldsymbol{E}_{11}(t) & 0 \\ 0 & \boldsymbol{E}_{22}(t) \end{bmatrix}}_{\boldsymbol{E}(t)} \underbrace{\begin{bmatrix} \mathbf{x}_1(t+\Delta t) \\ \mathbf{x}_2(t+\Delta t) \end{bmatrix}}_{\mathbf{x}(t+\Delta t)} = \underbrace{\begin{bmatrix} \boldsymbol{A}_{11}(t) & 0 \\ 0 & \boldsymbol{A}_{22}(t) \end{bmatrix}}_{\boldsymbol{A}(t)} \underbrace{\begin{bmatrix} \mathbf{x}_1(t) \\ \mathbf{x}_2(t) \end{bmatrix}}_{\mathbf{x}(t)} + \underbrace{\begin{bmatrix} \boldsymbol{B}_{11}(t) & 0 \\ 0 & \boldsymbol{B}_{22}(t) \end{bmatrix}}_{\boldsymbol{B}(t)} \underbrace{\begin{bmatrix} \mathbf{u}_1(t) \\ \mathbf{u}_2(t) \end{bmatrix}}_{\mathbf{u}(t)} + \mathbf{f}(\mathbf{x}_1, \mathbf{x}_2, t) \tag{1a}$$

$$\underbrace{\begin{bmatrix} \mathbf{y}_1(t) \\ \mathbf{y}_2(t) \end{bmatrix}}_{\mathbf{y}(t)} = \underbrace{\begin{bmatrix} \boldsymbol{C}_{11}(t) & 0 \\ 0 & \boldsymbol{C}_{22}(t) \end{bmatrix}}_{\boldsymbol{C}(t)} \underbrace{\begin{bmatrix} \mathbf{x}_1(t) \\ \mathbf{x}_2(t) \end{bmatrix}}_{\mathbf{x}(t)} + \underbrace{\begin{bmatrix} \boldsymbol{D}_{11}(t) & 0 \\ 0 & \boldsymbol{D}_{22}(t) \end{bmatrix}}_{\boldsymbol{D}(t)} \underbrace{\begin{bmatrix} \mathbf{u}_1(t) \\ \mathbf{u}_2(t) \end{bmatrix}}_{\mathbf{u}(t)} \tag{1b}$$

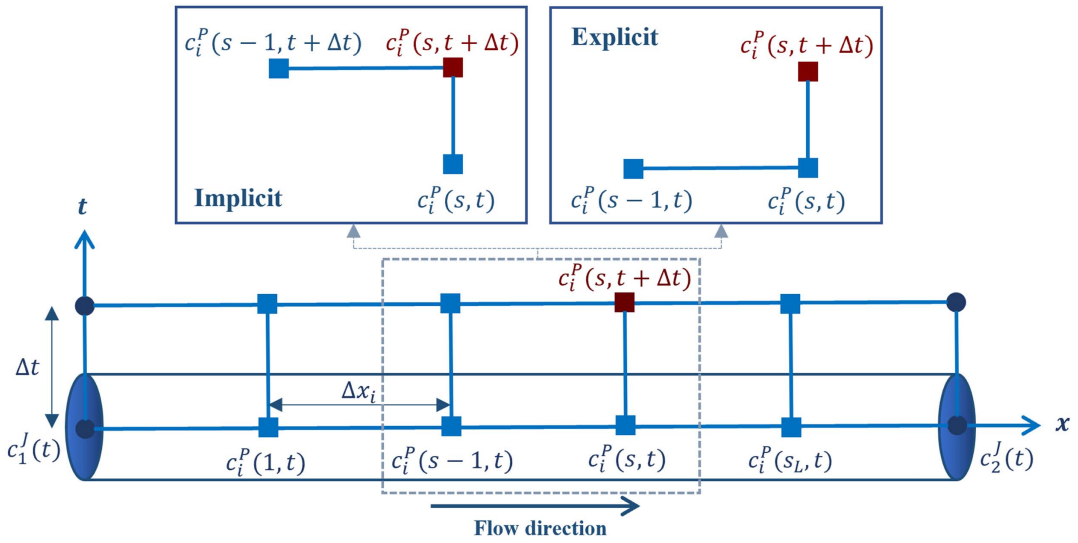

Fig. 2. Implicit and explicit upwind discretization schemes for Pipe i connecting Junctions 1 and 2. Each scheme calculates concentration $c_i^P(s,t+\Delta t)$ at segment s (colored in maroon) depending on concentrations at the segments and nodes included in its frame.

where variable t = specific time in a simulation period $[0, T_s]$; Δt = time step or sampling time; vectors $\mathbf{x}_1(t)$ and $\mathbf{x}_2(t) \in \mathbb{R}^{n_x}$ = concentrations of chlorine and the other fictitious reactant (two-species model) in the entire network; vector $\mathbf{u}_1(t) \in \mathbb{R}^{n_{u1}}$ = dosages of injected chlorine; vector $\mathbf{u}_2(t) \in \mathbb{R}^{n_{u2}}$ accounts for planned or unplanned injection of the fictitious component; vector $\mathbf{f}(\mathbf{x}_1, \mathbf{x}_2, t)$ encapsulates the nonlinear part of the equations representing the mutual nonlinear reaction between the two chemicals; vector $\mathbf{y}_1(t) \in \mathbb{R}^{n_{y1}}$ = sensor measurements of chlorine concentrations at specific locations in the network; and $\mathbf{y}_2(t) \in \mathbb{R}^{n_{y2}}$ captures the fictitious reactant measurements by sensors in the network if they exist. The state-space matrices $\{\boldsymbol{E}, \boldsymbol{A}, \boldsymbol{B}, \boldsymbol{C}, \boldsymbol{D}\}$. are all time-varying matrices that depend on the network topology and parameters, hydraulic parameters, decay rate coefficients for the disinfectant, and booster station and sensor locations. It is customary to assume these matrices evolve at a slower pace than the states $\mathbf{x}(t)$ and control inputs $\mathbf{u}(t)$. On another note, matrices $\boldsymbol{E}_{11}, \boldsymbol{E}_{22}$ change every hydraulic time step, allowing them to be represented at time t, not $t + \Delta t$ of the water quality simulation horizon.

The concentration evolution throughout network components is covered by the conservation of mass law, transport, decay, and reaction models of the substances. A full description of how the models are derived for each type of the components is provided in Elsherif et al. (2022). However, for the reader to be able to follow the developments of this paper, some material from Elsherif et al. (2022) needs to be reproduced and altered. We list a brief overview of the governing equations formulating our model and its state-space representation in the following sections.

Transport and Reaction in Pipes

Conservation of mass during transport and reaction in pipes is simulated by the 1D AR partial differential equation, which for Pipe i is expressed as

$$\partial_t c_i^{\mathrm{P}} = -v_i(t)\partial_x c_i^{\mathrm{P}} + R_{\mathrm{MS}}^{\mathrm{P}}(c_i^{\mathrm{P}}(x,t)) \tag{2}$$

where $c_i^{\mathrm{P}}(x,t)$ = concentration in the pipe at location x and time t; $v_i(t)$ = mean flow velocity; and $R_{\mathrm{MS}}^{\mathrm{P}}(c_i^{\mathrm{P}}(x,t))$ = multispecies reaction rate in pipes expression (more explanation is given in "Multispecies Reaction and Decay Model").

Eq. (2) is discretized over a fixed spatiotemporal grid, that for a Pipe i with length L_i is split into a number of segments $s_i = \lfloor L_i/(v_i(t)\Delta t) \rfloor$ of length $\Delta x_i = L_i/s_i$. In the considered 1D AR model, the two main processes are the advection where the concentration at a certain location and time is affected by upstream concentrations, and reaction where chemicals decay and/or mutually react. That being said, upwind discretization schemes are more descriptive to the actual physical process considered among other schemes (Hirsch 1990). Applying the Eulerian finite-difference (EFD)–based implicit upwind scheme on the multispecies water quality dynamics representation adapted in this paper has shown reliable results that trace chemicals' contractions within different networks with various scales, according to Elsherif et al. (2022). In this paper we consider both explicit and implicit upwind schemes to investigate their performance from a control–theoretic perspective (Fig. 2).

Explicit Upwind Scheme

For segment s of Pipe i except for the first segment, the concentration is calculated as

$$c_i^{\mathrm{P}}(s,t+\Delta t) = (1-\lambda_i(t))c_i^{\mathrm{P}}(s,t) + \lambda_i(t)c_i^{\mathrm{P}}(s-1,t) + R_{\mathrm{MS}}^{\mathrm{P}}(c_i^{\mathrm{P}}(s,t))\Delta t \tag{3}$$

where $\lambda_i(t) = (v_i(t)\Delta t)/\Delta x_i$ is the Courant number (CN) and, according to the Courant-Friedrichs-Lewy (CFL) condition, CN is maintained to be in the range of $0 < \lambda_i(t) \leq 1$ so the scheme is stable. Moreover, the concentrations in the first segment are expressed as in Eq. (4) assuming that the connecting upstream node is Junction j

$$c_i^{\mathrm{P}}(1,t+\Delta t) = (1-\lambda_i(t))c_i^{\mathrm{P}}(1,t) + \lambda_i(t)c_j^{\mathrm{J}}(t) + R_{\mathrm{MS}}^{\mathrm{P}}(c_i^{\mathrm{P}}(s,t))\Delta t \tag{4}$$

Implicit Upwind Scheme

The difference is that the concentration at the upstream segment or node is taken at the current time step. That is, Eq. (5*a*) calculates the

concentration for segment s of Pipe i. Also, the concentration of the first segment with Junction j as the upstream node is expressed in Eq. (5*b*)

$$(1+\lambda_i(t))c_i^{\mathrm{P}}(s,t+\Delta t)-\lambda_i(t)c_i^{\mathrm{P}}(s-1,t+\Delta t) = c_i^{\mathrm{P}}(s,t)+R_{\mathrm{MS}}^{\mathrm{P}}(c_i^{\mathrm{P}}(s,t))\Delta t \quad (5a)$$

$$(1+\lambda_i(t))c_i^{\mathrm{P}}(1,t+\Delta t)-\lambda_i(t)c_j^{\mathrm{J}}(t+\Delta t) = c_i^{\mathrm{P}}(1,t)+R_{\mathrm{MS}}^{\mathrm{P}}(c_i^{\mathrm{P}}(1,t))\Delta t \quad (5b)$$

Mass Balance at Network Components

For components other than pipes, conservation of mass is applied to formulate expressions for concentrations calculation.

Mass Balance at Reservoir

Reservoirs are assumed to have constant concentrations. For each Reservoir i, concentration is expressed as $c_i^{\mathrm{R}}(t+\Delta t)=c_i^{\mathrm{R}}(t)$.

Mass Balance at Pumps and Valves

The model deals with pumps and valves as transmission links with concentration equal to the concentration of the node upstream. That being said, for Pump i or Valve j installed after Reservoir k (as an example), concentrations are expressed as $c_i^{\mathrm{M}}(t+\Delta t)=c_k^{\mathrm{R}}(t+\Delta t)$ and $c_j^{\mathrm{V}}(t+\Delta t)=c_k^{\mathrm{R}}(t+\Delta t)$.

Mass Balance at Junctions

Chemicals are assumed to have complete and instantaneous mixing in junctions with no storage time. Thus, chemical concentration at each Junction i is expressed as

$$c_i^{\mathrm{J}}(t)=\frac{\sum_{j\in L_{\mathrm{in}}} q_{\mathrm{in}}^j(t)c_{\mathrm{in}}^j(t)+q_i^{\mathrm{B_J}}(t)c_i^{\mathrm{B_J}}(t)}{q_i^{\mathrm{D_J}}(t)+\sum\limits_{k\in L_{\mathrm{out}}} q_{\mathrm{out}}^k(t)} \quad (6)$$

where j and k = counters for total L_{in} links flowing into the junction and L_{out} links extracting flow from the junction; $q_{\mathrm{in}}^j(t)$ and $q_{\mathrm{out}}^k(t)$ = inflows and outflows from these links connected to the junction; $c_{\mathrm{in}}^j(t)$ = concentration in the inflow solute; $q_i^{\mathrm{B_J}}(t)$ = flow injected to the junction with concentration $c_i^{\mathrm{B_J}}(t)$ by booster station if located; and $q_i^{\mathrm{D_J}}(t)$ = demand.

Mass Balance at Tanks

Mass conservation in tanks assumes complete instantaneous mixing of all inflows, outflows, and stored water following the continuously stirred tank reactor (CSTR) model

$$V_i^{\mathrm{TK}}(t+\Delta t)c_i^{\mathrm{TK}}(t+\Delta t) = V_i^{\mathrm{TK}}(t)c_i^{\mathrm{TK}}(t)+\sum_{j\in L_{\mathrm{in}}} q_{\mathrm{in}}^j(t)c_{\mathrm{in}}^j(t)\Delta t+V_i^{\mathrm{B_{TK}}}(t+\Delta t)c_i^{\mathrm{B_{TK}}}(t+\Delta t) - \sum_{k\in L_{\mathrm{out}}} q_{\mathrm{out}}^k(t)c_i^{\mathrm{TK}}(t)\Delta t+R_{\mathrm{MS}}^{\mathrm{TK}}(c_i^{\mathrm{TK}}(t))V_i^{\mathrm{TK}}(t)\Delta t \quad (7)$$

where $V_i^{\mathrm{B_{TK}}}(t+\Delta t)$ = volume injected to the tank with concentration $c_i^{\mathrm{B_{TK}}}(t+\Delta t)$ by booster station if located; and $R_{\mathrm{MS}}^{\mathrm{TK}}(c_i^{\mathrm{P}}(x,t))$ = multispecies reaction rate in tanks expression (refer to "Multispecies Reaction and Decay Model").

Multispecies Reaction and Decay Model

Dividing the model into decay and mutual reaction dynamics allows it to consider a substance with relatively different reaction rates than the decay rate and for the model to be less sensitive to the other reactants' concentrations. The decay model is a first-order model that depends on only chlorine concentration and constant decay rate. Hence, the chlorine decay reaction rates for Pipe i and Tank j are $k_i^{\mathrm{P}}=k_b+(2k_wk_f)/(r_{\mathrm{P}_i}(k_w+k_f))$, $k_j^{\mathrm{TK}}=k_b$, where k_b is the bulk reaction rate constant, k_w is the wall reaction rate constant, k_f is the mass transfer coefficient between the bulk flow and the pipe wall, and r_{P_i} is the pipe radius.

The mutual reaction model is expressed by second-order nonlinear ordinary differential equations (ODEs), which are discretized using the forward Euler method $c(t+\Delta t)-c(t)=-k_r\Delta t(c(t)\tilde{c}(t))$, $\tilde{c}(t+\Delta t)-\tilde{c}(t)=-k_r\Delta t(c(t)\tilde{c}(t))$, where $c(t)$, $\tilde{c}(t)$ are the concentrations for chlorine and fictitious reactant; and k_r is the mutual reaction rate between them. Eventually, reaction expressions for pipes and tanks are

$$R_{\mathrm{M}}^{\mathrm{P}}(c_i^{\mathrm{P}}(s,t))=-k_rc_i^{\mathrm{P}}(s,t)\tilde{c}_i^{\mathrm{P}}(s,t),\quad R_{\mathrm{M}}^{\mathrm{TK}}(c_j^{\mathrm{TK}}(t))=-k_r\tilde{c}_j^{\mathrm{TK}}(t)c_j^{\mathrm{TK}}(t) \quad (8a)$$

$$R_{\mathrm{M}}^{\mathrm{P}}(\tilde{c}_i^{\mathrm{P}}(s,t))=-k_rc_i^{\mathrm{P}}(s,t)\tilde{c}_i^{\mathrm{P}}(s,t),\quad R_{\mathrm{M}}^{\mathrm{TK}}(\tilde{c}_j^{\mathrm{TK}}(t))=-k_r\tilde{c}_j^{\mathrm{TK}}(t)c_j^{\mathrm{TK}}(t) \quad (8b)$$

A full description of the state-space matrices construction for the upwind discretization schemes and an example on a simple three-node network [consisting of reservoir, a pump, a junction, a pipe, and a tank (Fig. 6)] are included in Elsherif et al. (2022) for the reader's reference on how to formulate the representation for different network component. That study validates the utilization of these EFD discretization schemes and the model performance as mentioned in comparison to EPANET and its extension, EPANET-MSX (WQ multispecies simulation tool). The comparison is considered reliable because the governing laws and equations are the same for all network components in both models. EPANET + EPANET-MSX employs the Lagrangian time-driven method, dividing each pipe into changing-sized segments, while the adopted EFD schemes in our study work within a fixed grid, facilitating the construction of a state-space representation with finite dimensions. The drawback associated with these discretization schemes is the large dimensionality of the model. However, the main objectives of this study are to address this challenge by employing model order reduction techniques and to integrate the reduced-order multispecies model effectively into a time-efficient real-time feedback control algorithm, which are outlined and presented in detail in the next sections. On the other hand, coupling the EPANET + EPANET-MSX model with a real-time control algorithm is complex and presents challenges due to the need to handle changes in segment count and size per pipe at each simulation time step, as well as being familiar with and able to leverage and use their toolkits in the coding language used (i.e., MATLAB and Python).

In the next section, we investigate different MOR algorithms for Eq. (1).

Model Order Reduction and Transformation of MS-WQM

The state-space representations formulated in the previous section are in form of NDEs like Eq. (1) with large numbers of variables resulting from high-resolution spatiotemporal discretization. To reach the end goal of this paper, which is controlling chlorine levels for Eq. (1), we propose different methodologies to reduce the model order and showcase their limitations, accuracy, computational time, and robustness and sensitivity to initial conditions and

fictitious reactant type. That being said, we list full descriptions of the methods covered in our framework. We start with linearizing Eq. (1), then explain model order reduction and transformation for linearized and original nonlinear systems.

Model Linearization

The mutual reaction is expressed as a nonlinear term that can be linearized using Taylor series approximations (Apostol 1991). By linearizing around operating points $c_o, \tilde{c}_o$, the nonlinear term $R_M(c(t), \tilde{c}(t))$ for both chemicals is expressed as

$$\begin{aligned} R_{\mathrm{M}}(c(t), \tilde{c}(t)) &= -k_r(c_o\tilde{c}_o + c_o(\tilde{c}(t) - \tilde{c}_o) + \tilde{c}_o(c(t) - c_o)) \\ &= -k_r(c_o\tilde{c}_o + c_o\tilde{c}(t) - c_o\tilde{c}_o + \tilde{c}_o c(t) - \tilde{c}_o c_o) \\ &= -k_r(c_o\tilde{c}(t) + \tilde{c}_o c(t) - \tilde{c}_o c_o) \end{aligned} \tag{9}$$

For each of the chemicals, the mutual reaction after linearization is broken down to a term that depends on its concentration, a term that depends on the other chemical's concentration, and a constant. The general state-space representation in Eq. (1) has a block-diagonal matrix of $\boldsymbol{A}$ matrices with no dependency between the chemical except in the $\mathbf{f}$ function. That is, by applying linearization to the model, the state-space representation is updated to linear difference equations (LDEs)

$$\begin{aligned} &\underbrace{\begin{bmatrix} \boldsymbol{E}_{11}(t) & 0 \\ 0 & \boldsymbol{E}_{22}(t) \end{bmatrix}}_{\boldsymbol{E}(t)} \underbrace{\begin{bmatrix} \mathbf{x}_1(t+\Delta t) \\ \mathbf{x}_2(t+\Delta t) \end{bmatrix}}_{\mathbf{x}(t+\Delta t)} \\ &= \underbrace{\begin{bmatrix} \breve{\boldsymbol{A}}_{11}(t) & \breve{\boldsymbol{A}}_{12}(t) \\ \breve{\boldsymbol{A}}_{21}(t) & \breve{\boldsymbol{A}}_{22}(t) \end{bmatrix}}_{\breve{\boldsymbol{A}}(t)} \underbrace{\begin{bmatrix} \mathbf{x}_1(t) \\ \mathbf{x}_2(t) \end{bmatrix}}_{\mathbf{x}(t)} + \underbrace{\begin{bmatrix} \boldsymbol{B}_{11}(t) & 0 \\ 0 & \boldsymbol{B}_{22}(t) \end{bmatrix}}_{\boldsymbol{B}(t)} \underbrace{\begin{bmatrix} \mathbf{u}_1(t) \\ \mathbf{u}_2(t) \end{bmatrix}}_{\mathbf{u}(t)} \\ &+ \boldsymbol{\Phi} \end{aligned} \tag{10}$$

where $\breve{\boldsymbol{A}}_{11}(t)$ and $\breve{\boldsymbol{A}}_{22}(t)$ = modified diagonal matrices; $\breve{\boldsymbol{A}}_{12}(t)$ and $\breve{\boldsymbol{A}}_{21}(t)$ = matrices gathering the dependency between the two species concentrations; and $\boldsymbol{\Phi}$ = vector containing the constants. The changes in $\breve{\boldsymbol{A}}_{11}(t)$ and $\breve{\boldsymbol{A}}_{22}(t)$ from the original matrices are only in the submatrices and elements representing pipes and tanks only (i.e., $\boldsymbol{A}_{\mathrm{P}}^{\mathrm{P}}$ and $\boldsymbol{A}_{\mathrm{TK}}^{\mathrm{TK}}$).

Model Order Reduction and Transformation Algorithms

In our study, we investigate two SVD-based projection methods; POD and BPOD. The reason behind not applying the BT method is that it has been proven to be computationally impractical for the linear water quality model (Wang et al. 2022). Both POD and BPOD are applied on the linearized MS-WQM, while an extension to the POD method is applied to reduce the nonlinear model where the nonlinear term is directly evaluated (Fig. 3).

Before explaining the detailed approach of the aforementioned methods, we start by explaining the general approach of SVD-based methods where a snapshot of the original space is taken. For the general nonlinear state-space representation in Eq. (1) that can be concisely formulated as follows

$$\begin{aligned} \boldsymbol{E}(t)\mathbf{x}(t+\Delta t) &= \boldsymbol{A}(t)\mathbf{x}(t) + \boldsymbol{B}(t)\mathbf{u}(t) + \mathbf{f}(\mathbf{x}(t)) \\ \mathbf{y}(t) &= \boldsymbol{C}(t)\mathbf{x}(t) + \boldsymbol{D}(t)\mathbf{u}(t) \end{aligned} \tag{11}$$

the first step is to map the representation states $\mathbf{x} \in \mathbb{R}^{n_x}$ to another space state $\mathbf{w} \in \mathbb{R}^{n_x}$. This mapping aims to reorder the states according to their influence in the preserved property. Driven by the goal of applying the control algorithm on our model, we care to capture the most controllable and observable snapshots of the original space. Transformation is performed through constructing a nonsingular matrix $\boldsymbol{V} \in \mathbb{R}^{n_x \times n_x}$, so that $\mathbf{x} = \boldsymbol{V}\mathbf{w}$. That is, Eq. (11) is expressed in terms of $\mathbf{w}$ as follows:

$$\begin{aligned} \boldsymbol{E}_w(t)\mathbf{w}(t+\Delta t) &= \boldsymbol{A}_w(t)\mathbf{w}(t) + \boldsymbol{B}_w(t)\mathbf{u}(t) + \boldsymbol{V}^{-1}\mathbf{f}(\boldsymbol{V}\mathbf{w}(t)) \\ \mathbf{y}_w(t) &= \boldsymbol{C}_w(t)\mathbf{w}(t) + \boldsymbol{D}(t)\mathbf{u}(t) \end{aligned} \tag{12}$$

where $\boldsymbol{E}_w = \boldsymbol{V}^{-1}\boldsymbol{E}\boldsymbol{V}$; $\boldsymbol{A}_w = \boldsymbol{V}^{-1}\boldsymbol{A}\boldsymbol{V}$; $\boldsymbol{B}_w = \boldsymbol{V}^{-1}\boldsymbol{B}$; and $\boldsymbol{C}_w = \boldsymbol{C}\boldsymbol{V}$.

Next, the reduced-order model is captured from the transformed mapping with number of states $n_r \ll n_x$ denoted by $\mathbf{x}_r \in \mathbb{R}^{n_r}$. A snapshot is taken of $\mathbf{x}$ equal to $\boldsymbol{V}_r\mathbf{x}_r$, where $\boldsymbol{V}_r$ is the matrix composed of the first n_r columns of $\boldsymbol{V}$. Similarly, we define $\boldsymbol{L}_r$ as the first n_r rows of $\boldsymbol{V}^{-1}$. Finally, the reduced-order model is expressed as

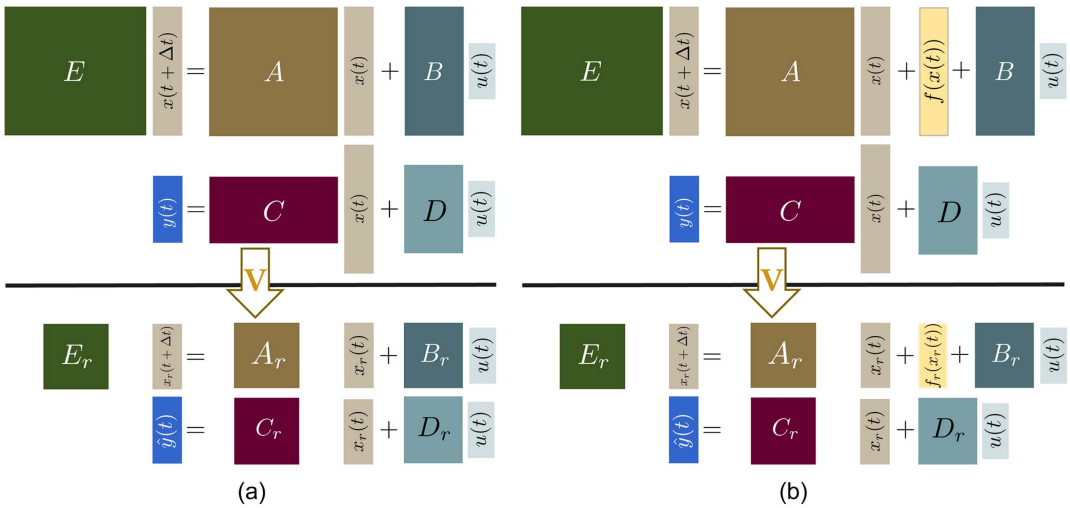

Fig. 3. (a) Linear; and (b) nonlinear MOR methods configuration.

J. Water Resour. Plann. Manage. 2024, 150(2): 04023077

$$\boldsymbol{E}_r(t)\mathbf{x}_r(t+\Delta t) = \boldsymbol{A}_r(t)\mathbf{x}_r(t) + \boldsymbol{B}_r(t)\mathbf{u}(t) + \mathbf{f}_r(\mathbf{x}_r(t))$$
$$\bar{\mathbf{y}}_r(t) = \boldsymbol{C}_r(t)\mathbf{x}_r(t) + \boldsymbol{D}(t)\mathbf{u}(t) \tag{13}$$

where $\boldsymbol{E}_r = \boldsymbol{L}_r\boldsymbol{E}\boldsymbol{V}_r$; $\boldsymbol{A}_r = \boldsymbol{L}_r\boldsymbol{A}\boldsymbol{V}_r$; $\boldsymbol{B}_r = \boldsymbol{L}_r\boldsymbol{B}$; and $\boldsymbol{C}_r = \boldsymbol{C}\boldsymbol{V}_r$.

The choice of n_r can be done arbitrarily as a fixed number or to conserve a specified level of energy between ROM and FOM. The energy of a system is determined by the summation of its eigenvalues; hence, n_r can be chosen to keep a certain energy percentage of FOM in ROM (Lall et al. 1999). However, we investigate choosing different numbers of n_r for each case study where the energy persevered is increased with larger n_r.

Additionally, the majority of MOR methods deal with original systems with zero initial conditions, which does not align with the nature of water quality dynamics. Previously, Wang et al. (2022) dealt with that by recognizing the nonzero initials network-wide as inputs for the system and setting $\hat{\mathbf{x}}(t) = \mathbf{x}(t) - \mathbf{x}(0)$ in the original model. We follow same approach with further analysis for the nonlinear term of the mutual dynamics. The mutual reaction dynamics as stated in "Multispecies Reaction and Decay Model" take place in pipes and tanks. That is, vector $\mathbf{f}$ contains zeros except for states of pipes' segments and tanks. We define $\mathbf{x}_{\mathrm{MS}_1}(t) \coloneqq \{c^{\mathrm{TK}}(t), c^{\mathrm{P}}(t)\}$ and $\mathbf{x}_{\mathrm{MS}_2}(t) \coloneqq \{\tilde{c}^{\mathrm{TK}}(t), \tilde{c}^{\mathrm{P}}(t)\}$. Accordingly

$$\mathbf{f}(\mathbf{x}_{\mathrm{MS}_1}(t), \mathbf{x}_{\mathrm{MS}_2}(t)) = \boldsymbol{\alpha} \cdot \mathbf{x}_{\mathrm{MS}_1}(t) \cdot \mathbf{x}_{\mathrm{MS}_2}(t) \tag{14}$$

where $\boldsymbol{\alpha} \coloneqq \{\boldsymbol{\alpha}_{\mathrm{TK}}, \boldsymbol{\alpha}_{\mathrm{P}}\}$; $\alpha_j^{\mathrm{TK}} = -k_r\Delta t\{V_j^{\mathrm{TK}}(t)/[V_j^{\mathrm{TK}}(t+\Delta t)]\}\ \forall\ j = 1, \ldots, n_{\mathrm{TK}}$; and $\alpha_l^{\mathrm{P}} = -k_r\Delta t\ \forall\ l = 1, \ldots, \sum_{i=1}^{n_{\mathrm{P}}} s_{L_i}$.

Henceforward, by setting $\hat{\mathbf{x}}_{\mathrm{MS}_1}(t) = \mathbf{x}_{\mathrm{MS}_1}(t) - \mathbf{x}_{\mathrm{MS}_1}(0)$ and $\hat{\mathbf{x}}_{\mathrm{MS}_2}(t) = \mathbf{x}_{\mathrm{MS}_2}(t) - \mathbf{x}_{\mathrm{MS}_2}(0)$ and substituting into Eq. (14), we get

$$\begin{aligned}
&\mathbf{f}(\hat{\mathbf{x}}_{\mathrm{MS}_1}(t), \hat{\mathbf{x}}_{\mathrm{MS}_2}(t)) \\
&\quad = \boldsymbol{\alpha} \bullet \hat{\mathbf{x}}_{\mathrm{MS}_1}(t) \bullet \hat{\mathbf{x}}_{\mathrm{MS}_2}(t) \\
&\quad = \boldsymbol{\alpha} \bullet (\mathbf{x}_{\mathrm{MS}_1}(t) - \mathbf{x}_{\mathrm{MS}_1}(0)) \bullet (\mathbf{x}_{\mathrm{MS}_2}(t) - \mathbf{x}_{\mathrm{MS}_2}(0)) \\
&\quad = \boldsymbol{\alpha} \bullet (\mathbf{x}_{\mathrm{MS}_1}(t) \bullet \mathbf{x}_{\mathrm{MS}_2}(t) - \mathbf{x}_{\mathrm{MS}_2}(0) \bullet \mathbf{x}_{\mathrm{MS}_1}(t) \\
&\qquad - \mathbf{x}_{\mathrm{MS}_1}(0) \bullet \mathbf{x}_{\mathrm{MS}_2}(t) + \mathbf{x}_{\mathrm{MS}_1}(0) \bullet \mathbf{x}_{\mathrm{MS}_2}(0))
\end{aligned} \tag{15}$$

which proves that considering $\mathbf{f}(\hat{\mathbf{x}}_{\mathrm{MS}_1}(t), \hat{\mathbf{x}}_{\mathrm{MS}_2}(t))$ can be utilized by updating $\boldsymbol{A}(t)$ in the original model to eliminate the negative terms for pipes and tanks, while the positive constant term encapsulates the nonlinear term at the initial concentrations, which is already considered. Subsequently, the full-order model is formulated as

$$\boldsymbol{E}(t)\hat{\mathbf{x}}(t+\Delta t) = \hat{\boldsymbol{A}}(t)\hat{\mathbf{x}}(t) + \hat{\boldsymbol{B}}(t)\hat{\mathbf{u}}(t) + \mathbf{f}(\hat{\mathbf{x}}(t))$$
$$\mathbf{y}(t) = \boldsymbol{C}(t)\hat{\mathbf{x}}(t) + \hat{\boldsymbol{D}}(t)\hat{\mathbf{u}}(t) \tag{16}$$

where

$$\hat{\boldsymbol{A}}(t) = \begin{bmatrix} \boldsymbol{A}_{11}(t) & \hat{\boldsymbol{A}}_{12}(t) \\ \hat{\boldsymbol{A}}_{21}(t) & \boldsymbol{A}_{22}(t) \end{bmatrix}$$

$\hat{\boldsymbol{B}}(t) = [\boldsymbol{B}(t) \quad \boldsymbol{A}(t)\mathbf{x}(0)]$; $\hat{\boldsymbol{D}}(t) = [\boldsymbol{D}(t) \quad \boldsymbol{C}(t)\mathbf{x}(0)]$; and $\hat{\mathbf{u}}(t) = [\mathbf{u}^{\intercal}(t) \quad \mathbf{1}^{\intercal}]^{\intercal}$.

On the other hand, for the linearized full-order model in Eq. (10), the same approach as in Wang et al. (2022) is followed and the final model formulated as

$$\boldsymbol{E}(t)\hat{\mathbf{x}}(t+\Delta t) = \hat{\boldsymbol{A}}(t)\hat{\mathbf{x}}(t) + \hat{\boldsymbol{B}}(t)\hat{\mathbf{u}}(t) + \boldsymbol{\Phi}$$
$$\mathbf{y}(t) = \boldsymbol{C}(t)\hat{\mathbf{x}}(t) + \hat{\boldsymbol{D}}(t)\hat{\mathbf{u}}(t) \tag{17}$$

where $\hat{\boldsymbol{A}}(t) = \breve{\boldsymbol{A}}(t)$; $\hat{\boldsymbol{B}}(t) = [\boldsymbol{B}(t) \quad \breve{\boldsymbol{A}}(t)\mathbf{x}(0)]$; $\hat{\boldsymbol{D}}(t) = [\boldsymbol{D}(t) \quad \boldsymbol{C}(t)\mathbf{x}(0)]$; and $\hat{\mathbf{u}}(t) = [\mathbf{u}^{\intercal}(t) \quad \mathbf{1}^{\intercal}]^{\intercal}$.

Last, we judge the performance of the MOR methods by calculating the root-mean-square error (RMSE) metric

$$\mathrm{RMSE} = \sqrt{\frac{1}{N_p}\sum_{j=1}^{N_p} \|\mathbf{y}(j) - \bar{\mathbf{y}}(j)\|_2^2} \tag{18}$$

The error is calculated for a specific simulation period of N_p time steps through which we apply the same system inputs $\mathbf{u}(j)$ to the two models.

In the following sections, we give a full description of the utilized methods. We start with applying POD and BPOD for the linearized formulation of the system, followed by integrating and handling the nonlinearity in the original representation of the system [Eq. (1) for the case of zero initial conditions and Eq. (16) for the case of nonzero initial conditions].

The basic and the balanced POD methods are considered data-driven SVD methods. The main idea is to build empirical Gramians based on snapshots of the original system. These empirical Gramians avoid solving complicated, in many cases intractable, Lyapunov equations. The POD method relies on constructing a controllability Gramian, while BPOD constructs finite horizon controllability and observability Gramians. Notably, the POD method favors highly controllable states over highly observable but less controllable ones, which BPOD averts by reflecting observability in the captured snapshot.

In our system, the concepts of controllability and observability for the two chemicals are different in what they reflect. While the input vector $\mathbf{u}_1(t)$ depicts chlorine injections into the system by source or rechlorination stations, vector $\mathbf{u}_2(t)$ enables simulating the intrusion of the contaminant to the system (Diao and Rauch 2013). Henceforward, controllability for the second chemical indicates which network components get exposed or affected by the contamination event. On the other hand, typically water quality sensors are located to measure chlorine levels which defines the abstract concept of the system being observable for water quality measurements. This is a main reason for chlorine monitoring to be a solid proxy of the water quality state in a specific network. However, no sensors are placed for contaminants detection specifically with the wide range of types and characteristics of those contaminants. That is, contaminant's observability is reflected in chlorine levels and not quantifiable in the matrix $\boldsymbol{C}_{22}$ of Eq. (1*b*) (i.e., a zero matrix). That puts a limitation on applying the BPOD method because it overlooks this contaminant because it is not observable. In "Balanced Proper Orthogonal Decomposition," we propose a special approach to solve this issue. In addition, with no output measurement for that chemical, the RMSE metric in Eq. (18) only measures the error for chlorine. In fact, the main purpose of this work is to control and monitor chlorine under contamination events, which makes it valid to focus on the output of measuring its concentrations that are accurately representing the real-time state. Nevertheless, to evaluate the performance of the applied MOR methods, we assume the existence of imaginary sensors on some specific nodes to measure the fictitious reactant concentrations to calculate the corresponding error.

In the following subsections, we explain what snapshots each method captures and how to construct these Gramians correspondingly.

Proper Orthogonal Decomposition

This method captures snapshot matrix $\boldsymbol{X}_m$ that is built for specific number of steps m by concatenating the states vector into

$$\boldsymbol{X}_m = [\,\mathbf{x}(0), \quad \mathbf{x}(1), \ldots, \mathbf{x}(m-1)\,] \tag{19}$$

where $\boldsymbol{X} \in \mathbb{R}^{n_x \times m}$.

The approximate m-step controllability Gramian $\boldsymbol{W}_{C_m}$ is defined as $\boldsymbol{X}_m \boldsymbol{X}_m^{\intercal} \in \mathbb{R}^{n_x \times n_x}$. Next, we apply eigenvalue decomposition (ED) $\boldsymbol{W}_{C_m} \boldsymbol{V} = \boldsymbol{V}\boldsymbol{\Lambda}$ and obtain $\boldsymbol{V}$, whose columns are the corresponding eigenvectors. However, in many cases applying ED for an $n_x \times n_x$ matrix with large n_x is taxing. This can be avoided in cases of $m \ll n_x$ by constructing $\tilde{\boldsymbol{W}}_{C_m} = \boldsymbol{X}_m^{\intercal} \boldsymbol{X}_m \in \mathbb{R}^{m \times m}$. Accordingly, the eigenvalue decomposition procedure is easier and requires less computational time (Luchtenburg and Rowley 2011). In this case, ED is formulated as $\tilde{\boldsymbol{W}}_{C_m} \boldsymbol{Q} = \boldsymbol{Q}\boldsymbol{\Lambda}$, where $\boldsymbol{\Lambda}$ is the diagonal matrix of eigenvalues and matrix $\boldsymbol{Q}$ is assembled with eigenvectors as columns. The transformation matrix is then calculated as $\boldsymbol{V} = \boldsymbol{X}_m \boldsymbol{Q} \boldsymbol{\Lambda}^{-1/2}$. For a detailed step-by-step depiction of the POD method, follow Procedure 1. This procedure is followed for both chemicals.

Procedure 1. POD for general MS-WQM

1. Construct snapshot $\boldsymbol{X}_m$ as in Eq. (19)
2. **if** $n_x \ll m$ **then**
3. Calculate $\boldsymbol{W}_{C_m} = \boldsymbol{X}_m \boldsymbol{X}_m^{\intercal}$
4. Obtain transformation matrix $\boldsymbol{V}$ by applying eigenvalue decomposition $\boldsymbol{W}_{C_m} \boldsymbol{V} = \boldsymbol{V}\boldsymbol{\Lambda}$
5. **else**
6. Calculate $\tilde{\boldsymbol{W}}_{C_m} = \boldsymbol{X}_m^{\intercal} \boldsymbol{X}_m$
7. Obtain matrices forms of eigenvector and eigenvalue of $\tilde{\boldsymbol{W}}_{C_m}$, $\boldsymbol{Q}$ and $\boldsymbol{\Lambda}$
8. Calculate transformation matrix as $\boldsymbol{V} = \boldsymbol{X}_m \boldsymbol{Q} \boldsymbol{\Lambda}^{-1/2}$
9. **end if**
10. Specify n_r
11. Define $\boldsymbol{V}_r$ as the first n_r columns of $\boldsymbol{V}$
12. Define $\boldsymbol{L}_r$ as the first n_r rows of $\boldsymbol{V}^{-1}$
13. Calculate $\boldsymbol{E}_r, \boldsymbol{A}_r, \boldsymbol{B}_r$, and $\boldsymbol{C}_r$
14. **if** FOM is nonlinear **then**
15. Follow Procedure 2
16. **end if**

Mapping and Integrating the Nonlinearity

While applying MOR, the reason behind separating the linear term(s) and the nonlinear term(s) is to be able to capture the behavior of the latter while working in a subspace of the original system (i.e., $\mathcal{R}^{n_r}$ instead of $\mathcal{R}^{n_x}$). In Eq. (13), following the projection of the whole system the nonlinear term is expressed as $\mathbf{f}_r = \boldsymbol{L}_r \mathbf{f}(\boldsymbol{V}_r \mathbf{x}_r(t))$. Yet, the computational complexity of the nonlinear term still depends on n_x

$$\mathbf{f}_r = \underbrace{\boldsymbol{L}_r}_{n_r \times n_x} \underbrace{\mathbf{f}(\boldsymbol{V}_r \mathbf{x}_r(t))}_{n_x \times 1}$$

Henceforward, it is proposed to reduce the nonlinear term based on an approximate hyper-reduction approach. The approach is to measure not the full state-space variables, but particular points and from those points we construct the nonlinear term by interpolation around these points. In our study we specify the number of these points to equal n_r

$$\mathbf{f}_r = \underbrace{\boldsymbol{L}_r \boldsymbol{U}_{f_r}}_{n_r \times n_r} \underbrace{\hat{\mathbf{f}}(t)}_{n_r \times 1}$$

The goal is to project $\mathbf{f}(\boldsymbol{V}_r \mathbf{x}_r(t))$ onto $\boldsymbol{U}_{f_r}$ so that $\mathbf{f}(\boldsymbol{V}_r \mathbf{x}_r(t)) \approx \boldsymbol{U}_{f_r} \hat{\mathbf{f}}(t)$ and $\boldsymbol{L}_r \boldsymbol{U}_{f_r}$ can be precomputed offline. This approach is called the gappy method of Galerkin projection and the DEIM is used to reconstruct the nonlinear vector by interpolation. We adopt a greedy sampling algorithm to construct the measurement matrix to select the entries used.

We start by stacking numerical snapshot $\boldsymbol{F}_m$ only for the nonlinear term

$$\boldsymbol{F}_m = [\,\mathbf{f}(\mathbf{x}(0)), \quad \mathbf{f}(\mathbf{x}(1)), \ldots, \mathbf{f}(\mathbf{x}(m-1))\,] \tag{20}$$

followed by performing a separate SVD for that snapshot, $\boldsymbol{F}_m = \boldsymbol{U}_f \boldsymbol{\Sigma}_F \boldsymbol{Q}_f^{\intercal}$. The next step is to define a rank n_r approximating basis $\boldsymbol{U}_{f_r}$ as the first n_r columns of $\boldsymbol{U}_f$. Next, we construct the measurement matrix $\boldsymbol{K}$ by applying the greedy sampling algorithm as summarized in Procedure 2. As shown in Fig. 4, the greedy sampling algorithm starts by choosing the index with the maximum value in the first mode $\mathbf{u}_1$ and making it the first measurement location. In the second and subsequent iterations, we compute the residual to evaluate how the current measurement subspace projects onto the next one and decide on the next measurement point. The reason behind choosing the measurement with the maximum residual is that the modes are no longer orthogonal in the support space; hence, we calculate the residuals and locate the index with the maximum residual.

Procedure 2. Nonlinearity handling in MOR

1 Capture $\boldsymbol{F}_m$ as in Eq. (20)
2 Perform SVD of $\boldsymbol{F}_m = \boldsymbol{U}_f \boldsymbol{\Sigma}_F \boldsymbol{Q}_f^{\intercal}$
3 Construct $\boldsymbol{U}_{f_r}$ as the first n_r columns of $\boldsymbol{U}_f$
4 **Start** greedy sampling algorithm for selecting the indexes (entries of $\mathbf{f}$)
5 **Input:** $\boldsymbol{U}_{f_r} = [\mathbf{u}_1, \ldots, \mathbf{u}_{n_r}]$
6 **Output:** $\mathcal{I} \coloneqq \{i_1, \ldots, i_{n_r}\}$ and $\boldsymbol{K} = [\mathbf{e}_{i_1}, \ldots, \mathbf{e}_{i_r}]$
7 $[s, i_1] = \max\{|\mathbf{u}_1|\}$
8 $\boldsymbol{U}_{f_r} = [\mathbf{u}_1], \boldsymbol{K} = [\mathbf{e}_{i_1}]$
9 **for** $I = 2 : n_r$ **do**
10 solve $\boldsymbol{K}^{\intercal} \boldsymbol{U}_{f_r} \mathbf{b} = \boldsymbol{K}^{\intercal} \mathbf{u}_I$ for $\mathbf{b}$
11 $\mathbf{q} = \mathbf{u}_I - \boldsymbol{U}_{f_r} \mathbf{b}$
12 $[s, i_I] = \max\{|\mathbf{q}|\}$
13 $\boldsymbol{U}_{f_r} = [\boldsymbol{U}_{f_r}, \mathbf{u}_I]$, $\boldsymbol{K} = [\boldsymbol{K}, \mathbf{e}_{i_I}]$
14 **end for**
15 **Proceed**
16 Calculate $\hat{\mathbf{f}}(t) = (\boldsymbol{K}^{\intercal} \boldsymbol{U}_{f_r})^{-1} \mathbf{f}(\boldsymbol{K}^{\intercal} \boldsymbol{V}_r \mathbf{x}_r(t))$

Balanced Proper Orthogonal Decomposition

The advance in the BPOD method is the reflection of both controllability and observability in ranking the states, unlike POD. This is attained by constructing two snapshots of the system: $\tilde{\boldsymbol{X}}_m$, which captures the impulse responses when applying impulse signal as system input [i.e., $u_i(m) = \gamma(m)$], and $\boldsymbol{P}_m$, which is assembled from states $\mathbf{p}(t)$ obtained from the adjoint system with impulse response in the measurements as the system's output. For the linearized model in Eq. (17), the adjoint system can be expressed as follows:

$$\mathbf{p}(t + \Delta t) = \breve{\boldsymbol{A}}^{\intercal}(t)(\boldsymbol{E}^{-1}(t))^{\intercal} \mathbf{p}(t) + \boldsymbol{C}^{\intercal}(t) \mathbf{y}(t) + \boldsymbol{E}^{-1}(t) \boldsymbol{\Phi} \tag{21}$$

The next step is performing SVD to the block Hankel matrix $\boldsymbol{H}_m = \boldsymbol{P}_m^{\intercal} \tilde{\boldsymbol{X}}_m = \boldsymbol{U} \boldsymbol{\Sigma} \boldsymbol{Q}^{\intercal}$ then specifying n_r to collect the largest n_r singular values in $\boldsymbol{\Sigma}$ and obtain the corresponding left and right singular vectors (i.e., $\boldsymbol{U}_r$ and $\boldsymbol{Q}_r$). Accordingly, $\boldsymbol{V}_r$ and $\boldsymbol{S}_r$ are calculated as

$$\boldsymbol{V}_r = \tilde{\boldsymbol{X}}_m \boldsymbol{Q}_r \boldsymbol{\Sigma}_r^{1/2}, \qquad \boldsymbol{L}_r = \boldsymbol{\Sigma}_r^{1/2} \boldsymbol{U}_r^{\intercal} \boldsymbol{P}_m^{\intercal} \tag{22}$$

J. Water Resour. Plann. Manage., 2024, 150(2): 04023077

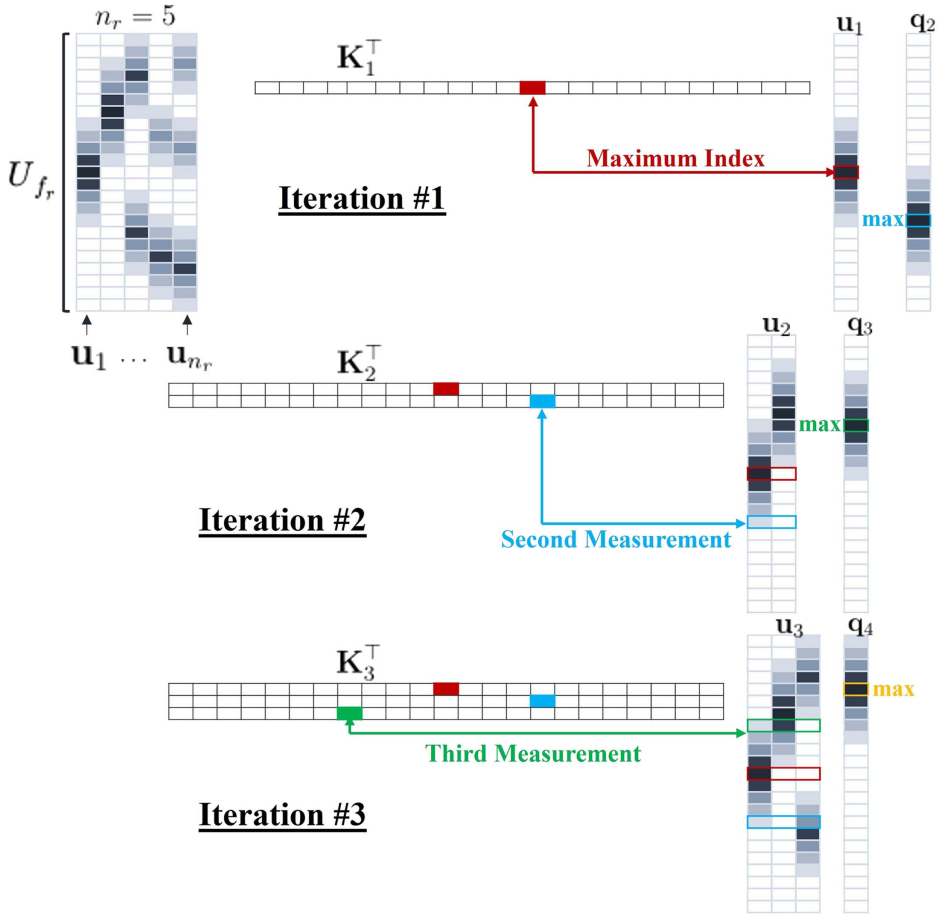

Fig. 4. Applying the greedy sampling algorithm to construct the measurement matrix $\boldsymbol{K}$ for the case of $n_r = 5$.

This approach is applicable for chlorine with sensors placed to measure its levels. For the fictitious reactant representing the contaminant, matrix $\boldsymbol{C}_{22}$ in Eq. (1*b*) is a zero matrix representing nonsensed variables in our system. To solve this issue, we assume the contamination event is detected and the source location is determined. This is considered a valid assumption in water quality monitoring to work backward detecting, classifying, and quantifying using conventional WQ sensors (Yang et al. 2009). This is different from the aforementioned imaginary sensors while calculating the error to evaluate the performance of the applied methods.

Another advance of the BPOD is the ability to stabilize it by choosing the length of the snapshots to be large enough to represent the actual Gramians shooting for infinity. We adopt an a priori stabilization method to ensure the snapshot captures the chemicals' evolution from the time it is injected in the system until it is observed by the furthest sensor. This is fulfilled by assembling the snapshots over a period exceeding, $\underline{m} = \max\left(\lceil T_{BS}/\Delta t \rceil\right) = \max\left(\lceil \sum L_i^{BS}/(v_i^{BS}\Delta t) \rceil\right)$ where L_i^{BS} and v_i^{BS} are the length and velocity of the pipes the chemical travels through a booster station to the furthest sensor. With the existence of multiple booster stations and sensors and within the simulation period, $\underline{m}$ is taken as the length corresponding to the maximum travel time T_{BS}. Accordingly, this method is affected by the actuators' and sensors' locations along the network. Last, Procedure 3 summarizes all the steps needed for a linear(ized) WQ model.

Procedure 3. BPOD for linear(ized) WQM

1 Obtain snapshots length $m = \underline{m}$
2 Construct snapshot $\tilde{\boldsymbol{X}}_m$ and $\boldsymbol{P}_m$
3 Construct the block Hankel matrix $\boldsymbol{H}_m = \boldsymbol{P}_m^\intercal \tilde{\boldsymbol{X}}_m$
4 Perform SVD of $\boldsymbol{H}_m = \boldsymbol{U}\boldsymbol{\Sigma}\boldsymbol{Q}^\intercal$
5 Specify n_r
6 Obtain $\boldsymbol{U}_r, \boldsymbol{\Sigma}_r$, and $\boldsymbol{Q}_r$
7 Calculate $\boldsymbol{V}_r$ and $\boldsymbol{L}_r$ via Eq. (22)
8 Calculate $\boldsymbol{E}_r, \boldsymbol{A}_r, \boldsymbol{B}_r$, and $\boldsymbol{C}_r$

Real-Time Regulation of MS-WQM via Model Predictive Control and McCormick Relaxation

The water quality control problem is formulated over simulation period $[0, T_s]$ and constrained by putting standard upper and lower bounds on chlorine concentrations stated by EPA regulations (Acrylamide 2009), which are $x_1^{\min} = 0.2$ mg/L and $x_1^{\max} = 4$ mg/L. The contaminant in the system is assumed to be detected and classified. Accordingly, for some toxic or health-threatening substances, a constraint can be introduced to be kept lower than the allowed concentration defined by the EPA. These lower and upper bounds for both chemicals formulates the constraint $\mathbf{x}^{\min} \le \mathbf{x}(t) \le \mathbf{x}^{\max}$. Additionally, the control inputs for chlorine are constrained to be nonnegative and limited by the chlorine availability and capacity of each booster station. The objective of this control problem is to keep chemicals concentrations in all the

J. Water Resour. Plann. Manage. 2024, 150(2): 04023077

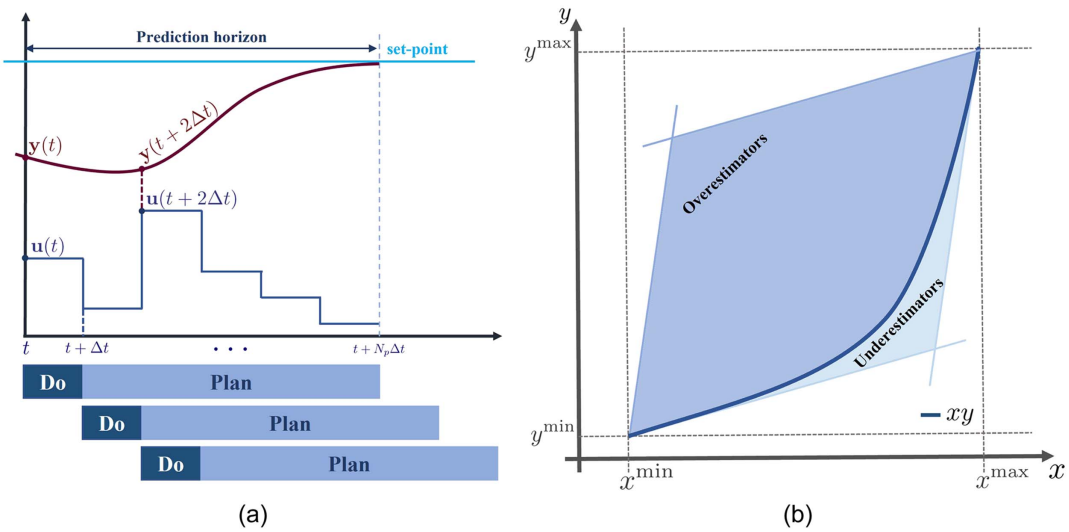

Fig. 5. (a) Discrete MPC prediction horizon scheme; and (b) McCormick envelope relaxation.

network's components within the aforementioned bounds while minimizing the cost of chlorine injections. That being said, the problem formulation is as follows:

$$\begin{aligned} \underset{\mathbf{x}(t),\mathbf{u}_1(t)}{\text{minimize}} \quad & \mathcal{J}(\mathbf{u}_1(t)) = \mu \sum_{t=1}^{N_p} \mathbf{q}^{\mathrm{B}}(t)^{\intercal}\mathbf{u}_1(t) \\ \text{subject to} \quad & \mathrm{WQM}(1) \\ & \mathbf{x}^{\min} \le \mathbf{x}(t) \le \mathbf{x}^{\max} \\ & \mathbf{u}_1^{\min} \le \mathbf{u}_1(t) \le \mathbf{u}_1^{\max} \end{aligned} \tag{23}$$

where problem variables $\mathbf{x}(t)$ and $\mathbf{u}_1(t)$ = chemicals concentrations network-wide and chlorine injections through booster stations; $\mathbf{q}^{\mathrm{B}}(t)$ = flow rates at the nodes corresponding to the locations of the booster stations; μ = unit cost of chlorine ($/mg); WQM = water quality model we are simulating and controlling following the representation in Eq. (1); and N_p = number of time steps in the simulation period, $N_p = T_p/\Delta t$.

Nonetheless, this problem has a large number of variables $\mathbf{x}(t)$ and $\mathbf{u}_1(t)$. This issue can be solved by transforming a constrained linear program (LP) in Eq. (23) to a quadratic program (QP) with fewer variables by applying real-time constrained model predictive control (WQ-MPC). The water quality control formulated in Wang et al. (2021) is based on the linear state-space representation of the single-species WQ dynamics. In addition, the same control algorithm is applied in Wang et al. (2022) for the reduced-order model of the single-species representation and it proved its validity and effectiveness. For brevity, we do not include the details and the derivation in this paper for the case of linearized MS-WQM. Eventually, the WQC problem is formulated as a quadratic program. For the nonlinear MS-WQM, the nonlinearity in the constraint can be relaxed using McCormick envelopes and integrated back to the original constrained control problem as explained in the following section.

McCormick Relaxation

The nonlinear term in the constraint is formulated as a bilinear expression depending on the concentration of two chemicals at a specific network component. This constraint can be relaxed using McCormick relaxation for bilinear nonlinear problems (McCormick 1976). This method turns the bilinear term into two envelopes surrounded by overestimators and underestimators to work within [Fig. 5(b)]. For a bilinear expression $z = x_1x_2$, where x_1 and x_2 are the two chemicals concentrations under $x_1^{\min} \le x_1 \le x_1^{\max}$ and $x_2^{\min} \le x_2 \le x_2^{\max}$, z is introduced as a new decision variable with the following constraints:

$$\begin{aligned} z &\ge x_1^{\min}x_2 + x_1x_2^{\min} - x_1^{\min}x_2^{\min} \\ z &\ge x_1^{\max}x_2 + x_1x_2^{\max} - x_1^{\max}x_2^{\max} \\ z &\le x_1^{\max}x_2 + x_1x_2^{\min} - x_1^{\max}x_2^{\min} \\ z &\le x_1^{\min}x_2 + x_1x_2^{\max} - x_1^{\min}x_2^{\max} \end{aligned} \tag{24}$$

In some cases, the upper bound on x_2 is not specified or its concentration initially is lower than the maximum allowed one stated by the EPA. In such cases, we specify $x_2^{\max}$ to be equal to this initial concentration detected to be able to tighten the overestimators' envelope while having the minimum equal to zero.

Eventually, the problem formulation explained for the linearized model can be adopted with these modifications. First, a new variable vector $\mathbf{z}(t)$ is introduced and it replaces $\mathbf{f}(\mathbf{x}_1, \mathbf{x}_2, t)$ in Eq. (1*a*). Additionally, the total number of the constraints added to the optimization problem via Eq. (24) is equal to $4(n_{\mathrm{TK}} + \sum_{i=1}^{n_{\mathrm{P}}} s_{L_i})$ because the nonlinear term is defined for pipes' segments and tanks and is the same for both chemicals at same element of the aforementioned [Eq. (8)]. To that end, the WQC problem described in Eq. (23) is modified as follows:

$$\begin{aligned} \underset{\mathbf{x}(t),\mathbf{u}_1(t),\mathbf{z}(t)}{\text{minimize}} \quad & \mathcal{J}(\mathbf{u}_1(t)) = \mu \sum_{t=1}^{N_p} \mathbf{q}^{\mathrm{B}}(t)^{\intercal}\mathbf{u}_1(t) \\ \text{subject to} \quad & \mathrm{WQM}(1) \\ & \mathbf{x}^{\min} \le \mathbf{x}(t) \le \mathbf{x}^{\max} \\ & \mathbf{u}_1^{\min} \le \mathbf{u}_1(t) \le \mathbf{u}_1^{\max} \\ & \mathrm{McCormick}(24) \end{aligned} \tag{25}$$

The next step is transforming Eq. (25) into a linear augmented formulation, based on which the final WQC-QP is built. First, by introducing $\mathbf{z}(t)$ into Eq. (1*a*), the state-space representation is updated as

$$\mathbf{x}(t+1) = \boldsymbol{A}(t)\mathbf{x}(t) + \boldsymbol{B}(t)\mathbf{u}(t) + \beta\mathbf{z}(t) \tag{26}$$

where $\beta = -k_r$. Then we define the change in the states and inputs as follows:

$$\Delta\mathbf{x}(t+1) = \mathbf{x}(t+1) - \mathbf{x}(t), \qquad \Delta\mathbf{u}(t+1) = \mathbf{u}(t+1) - \mathbf{u}(t),$$
$$\Delta\mathbf{z}(t+1) = \mathbf{z}(t+1) - \mathbf{z}(t) \tag{27}$$

To concatenate these rates of change in Eq. (26), $\Delta\mathbf{z}$ is assembled to the vector of systems decision inputs to be optimally chosen within the envelopes defined by Eq. (24). Eventually, we reach the augmented state-space representation in Eq. (28)

$$\underbrace{\begin{bmatrix}\Delta\mathbf{x}(t+1)\\ \mathbf{y}(t+1)\end{bmatrix}}_{\mathbf{x}_a(t+1)} = \underbrace{\begin{bmatrix}\boldsymbol{A}(t) & \mathbf{0}\\ \boldsymbol{C}(t)\boldsymbol{A}(t) & \boldsymbol{I}\end{bmatrix}}_{\boldsymbol{\Phi}_a}\underbrace{\begin{bmatrix}\Delta\mathbf{x}(t)\\ \mathbf{y}(t)\end{bmatrix}}_{\mathbf{x}_a(t)} + \underbrace{\begin{bmatrix}\boldsymbol{B}(t) & \beta\\ \boldsymbol{C}(t)\boldsymbol{B}(t) & \beta\boldsymbol{C}(t)\end{bmatrix}}_{\boldsymbol{\Gamma}_a}\underbrace{\begin{bmatrix}\Delta\mathbf{u}(t)\\ \Delta\mathbf{z}(t)\end{bmatrix}}_{\Delta\mathbf{u}_a(t)} \tag{28}$$

This augmented representation can be abstractly rewritten as $\mathbf{x}_a(t+1) = \boldsymbol{\Phi}_a\mathbf{x}_a(t+1) + \boldsymbol{\Gamma}_a\Delta\mathbf{u}_a(t)$. To avoid redundancy, integrating this equality into WQC-MPC formation follows the same approach of Wang et al. (2022) reaching the final QP [Wang et al. (2022), Eq. (38)]. On another note, the added constraints expressed in Eq. (24) are incorporated in the constraints on the optimization variables.

Table 1. Chlorine bulk decay and reaction models expressions

Model No.	Model	Model formulation	#States	L or NL[a]
M-1	First order	$\frac{dc}{dt} = -kc(t)$	n_x	L
M-2	First order with stable component	$\frac{dc}{dt} = -k(c(t) - c_{\mathrm{L}})$	n_x	L
M-3	Parallel first order	$\frac{dc_1}{dt}\|_{\mathrm{fast}} = -k_{\mathrm{fast}}c_1(t)$ $\frac{dc_2}{dt}\|_{\mathrm{slow}} = -k_{\mathrm{slow}}c_2(t)$ $c_i(t) = c_1(t) + c_2(t)$	$2n_x$	L
M-4	Parallel second order	$\frac{dc_{\mathrm{F}}}{dt}\|_{\mathrm{fast}} = -k_{\mathrm{fast}}c(t)c_{\mathrm{F}}(t)$ $\frac{dc_{\mathrm{S}}}{dt}\|_{\mathrm{slow}} = -k_{\mathrm{slow}}c(t)c_{\mathrm{S}}(t)$ $\frac{dc}{dt} = \frac{dc_{\mathrm{F}}}{dt} + \frac{dc_{\mathrm{S}}}{dt}$	$2n_x$	NL
M-5	nth order	$\frac{dc}{dt} = -kc^n(t)$	n_x	NL
M-6	nth order with stable component	$\frac{dc}{dt} = -k(c(t) - c_{\mathrm{L}})c^{(n-1)}$	n_x	NL
M-7	Second order with fictitious component	$\frac{dc}{dt} = -kc(t)\tilde{c}(t)$ $\frac{d\tilde{c}}{dt} = -kc(t)\tilde{c}(t)$	$2n_x$	NL
M-8	Second order with multiple components	$\frac{dc_i}{dt} = -k_ic(t)\tilde{c}_i(t)$ $\frac{d\tilde{c}_i}{dt} = -k_ic(t)\tilde{c}_i(t)$ $\frac{dc}{dt} = \sum_i^I \frac{dc_i}{dt}$	In_x	NL

[a]L = linear model expression; and NL = nonlinear model expression.

Generalized Comprehensive Water Quality Modeling and Control Framework

In our study, we have covered model order reduction and control for multispecies water quality dynamics where chlorine is reacting with another source of contamination in the form of a bilinear expression (refer to "Multispecies Reaction and Decay Model"). However, there are other formulations for single-species and multispecies chlorine bulk decay and reaction dynamics as listed in Elsherif et al. (2022). We include a short list of these formulations in Table 1; nevertheless, for more details and descriptions refer to the aforementioned study. The generalized framework described in Algorithm 1 maps out the methods adopted in this study to be applied on the different decay and reaction models.

For the first-order, first-order with stable component, and parallel first-order (M-1, M-2, and M-3) models, the dynamics are linear and accordingly follow the procedure of the linearized model represented in our study. The second order with multiple components (M-8) is considered to be the same formula as the second order with fictitious component (M-7) we cover in this paper except for the number of states that get multiplied by the number of reactants in the system. That is, model order reduction for M-8 becomes more demanded. On the other hand, the parallel second-order model (M-4) is a special form of the second order with fictitious component. Last, the nth order without and with stable component models are higher-order models that can be reduced as nonlinear models or be transferred into quadratic approximation and piecewise linear relaxation applied.

Algorithm 1. Generalized water quality modeling and control framework

Input: WDN topology, components' characteristics, and hydraulics parameters
Output: Real-time water quality states $\mathbf{x}(t)$ and control inputs $\mathbf{u}(t)$ at time t of a simulation period of T_s

Initialization
  Define Δt, number of segments s_i for each pipe and accordingly n_x
  Formulate WQ state-space representation Eq. (1) as explained in "State-Space Multispecies Water Quality Model" and according to the reaction dynamics in Table 1
Proceed
if *Applying M-1/M-2/M-3 reaction model* **then**
  Follow Procedure 3 to obtain ROM
  Apply constrained real-time WQ-MPC on Eq. (23)
else if *Applying M-4/M-7/M-8 reaction model* **then**
  if *Following Procedure 1* **then**
    Apply McCormick relaxation via Eq. (24)
    Apply constrained real-time WQ-MPC on Eq. (25)
  else
    Linearizing and following Procedure 3 **then**
    Apply constrained real-time WQ-MPC on Eq. (23)
  end if
else
  Applying M-5/M-6 **then**
  Follow Procedure 1 to obtain ROM
  Transform into quadratic approximation/Apply piecewise linear relaxation
  Apply constrained real-time WQ-MPC on Eq. (23)
end if

To recapitulate, this paper is an extension of Elsherif et al. (2022) and Wang et al. (2022). That is, some methods and aspects included in this section have already been covered in these studies.

Yet, we have decided to reintroduce this material in our study in a more concise way to ensure the reader can effectively follow and comprehend the new information being presented. In the following bullet points, we highlight the novelty in our work in comparison to these studies:

- A nonlinear multispecies water quality dynamics is adopted rather than the linear single-species dynamics in a control framework. These dynamics enable a heightened level of realism in the system dynamics representation.
- Two different paths are followed where different MOR methods and control algorithms are applied on the original nonlinear and linearized forms of the model. For the linearized model, we implement the same MOR techniques (specifically, POD and BPOD) described in Wang et al. (2022). On the other hand, for the nonlinear model, we introduce the gappy method, which employs a greedy algorithm to effectively handle the nonlinearity and reduce the model dimension.
- The implementation of these MOR techniques is expanded for the case of nonzero initial conditions by developing a closed formulation that preserves the original nonlinear formulation of the model.
- Likewise, for the linearized model, we implement the MPC algorithm explained in Wang et al. (2022) to control and regulate chlorine levels under the multispecies dynamics. In contrast, we extend the MPC algorithm to incorporate the McCormick relaxation technique, which is specifically tailored for the nonlinear model.
- While the same methods and algorithms are employed for the linearized model as in the linear single-species model described in Wang et al. (2022), special consideration is required when implementing these techniques for the linearized model. This is primarily due to the duplication of state numbers and the distinct construction of representation matrices for the fictitious reactant. These factors necessitate a specific approach to ensure accurate and reliable results during the implementation of these methods in the context of the linearized model.
- Explicit versus implicit discretization schemes are used to investigate and evaluate from a control–theoretic standpoint. Specifically, we apply upwind schemes, which offer a more accurate representation of the advection-reaction 1D PDEs compared to the Lax-Wendroff scheme utilized in Wang et al. (2022). The advance in implementing an upwind scheme is proven and demonstrated in Elsherif et al. (2022). In addition, the Lax-Wendroff scheme is an explicit scheme and the prior study does not extensively investigate the use of an implicit scheme in this context.
- A novel component of our study is investigating the water quality control framework performance under different system hydraulic settings. These settings directly impact the water quality dynamics and their progression over time within the same network. This exploration adds a unique dimension to our study, shedding light on the interplay between system hydraulics and water quality dynamics for enhanced understanding and improved control strategies.

The validity of these techniques and the performance of the control framework are evaluated and substantiated in the subsequent section through a series of numerical case studies.

Case Studies

This section demonstrates the proposed framework for model order reduction and control of MS-WQM. Particularly, we attempt to answer the following questions:

1. How does the number of operating points impact agreement between the linearized model and the nonlinear MS-WQM?
2. How effective are the proposed MOR producers in terms of accuracy and computational time when applied on the MS-WQM?
3. How sensitive is the performance of MOR and the control algorithm to the discretization methods and system's hydraulics?
4. How reliable and robust is model predictive control when applied to control chlorine levels under multispecies dynamics?

Numerical studies in this section are performed on three different networks: three-node, Net1, and FFCL-1 networks (Rossman et al. 2020). As shown in Fig. 6, the networks each have different topologies and scales. The three-node network is a self-designed network to help provide simple illustrations for different approaches throughout our framework implementation. Net1 includes different types of network components and has a looped layout. The FFCL-1 network is based on the Fairfield, California, water distribution system on which we test the scalability of our framework and its performance with scattered dead-ends. Also, Fig. 6 illustrates and lists each of the networks' components.

In addition to the listed components for each of the test networks in Fig. 6, each network has a different number of sensors and booster stations. The three-node network has one booster station at Junction J1 and one sensor at Tank TK1. Net1 has two stations at Junctions 1 and 6 and sensors at Junctions J4 and J9. Last, the controlled region of the FFCL-1 network has two sensors at Junctions J56 and J67, and one rechlorination station at J89.

For any WDN, the system dimension depends on the hydraulics parameters and water quality simulation time step, which accordingly define the number of segments for each pipe (i.e., pipe state variables). Further, changing the velocities and flows from one scenario to another results in distinct chemical concentrations across the network components for each. With that in mind, in some of our case studies we feature the effect of changing the hydraulics for the same network. In other case studies, we fix the hydraulics setting in the system to investigate or test a technique or an approach under discussion. In addition, for all studies performed in this section we use the implicit upwind scheme except for in "Implicit versus Explicit Discretization Schemes under Control–Theoretic Perspective," where we compare its performance with the explicit upwind scheme from a control–theoretic perspective.

Nonlinear versus Linearized Models

Studies (Chen 1999; Schilders et al. 2008; Liu and Barabási 2016) state that applying a linear MOR algorithm on a linearized system gives satisfactory performance when the linearized system is close to the original nonlinear one or operating within or near its linear regime. In these studies, linearization is performed around one operating point for the whole simulation horizon. We apply the same approach by linearizing around two operating points, (0, 0) and (0.2, 0.05) mg/L for chlorine and fictitious reactant, respectively, at Tank TK1 of the three-node network. In this scenario, a constant demand is drawn from J1 and sources of 2 mg/L of chlorine and 0.5 mg/L of the fictitious reactant are provided at R1 and zero initial conditions for other network components. As demonstrated in Fig. 7, linearization around the operating point of (0, 0) results in higher concentrations compared with the nonlinear model [based on the NDE in Eq. (1)] for both chemicals because it drops out the nonlinear term and neglects the mutual reaction. On the other hand, linearizing the model around one random operating point as (0.2, 0.05) mg/L results in relatively closer values for chlorine concentrations but not as close for the fictitious reactant. Furthermore, unlike this scenario, in real-time water networks hydraulics are not fixed and demands are time variant, resulting in chemical evolution

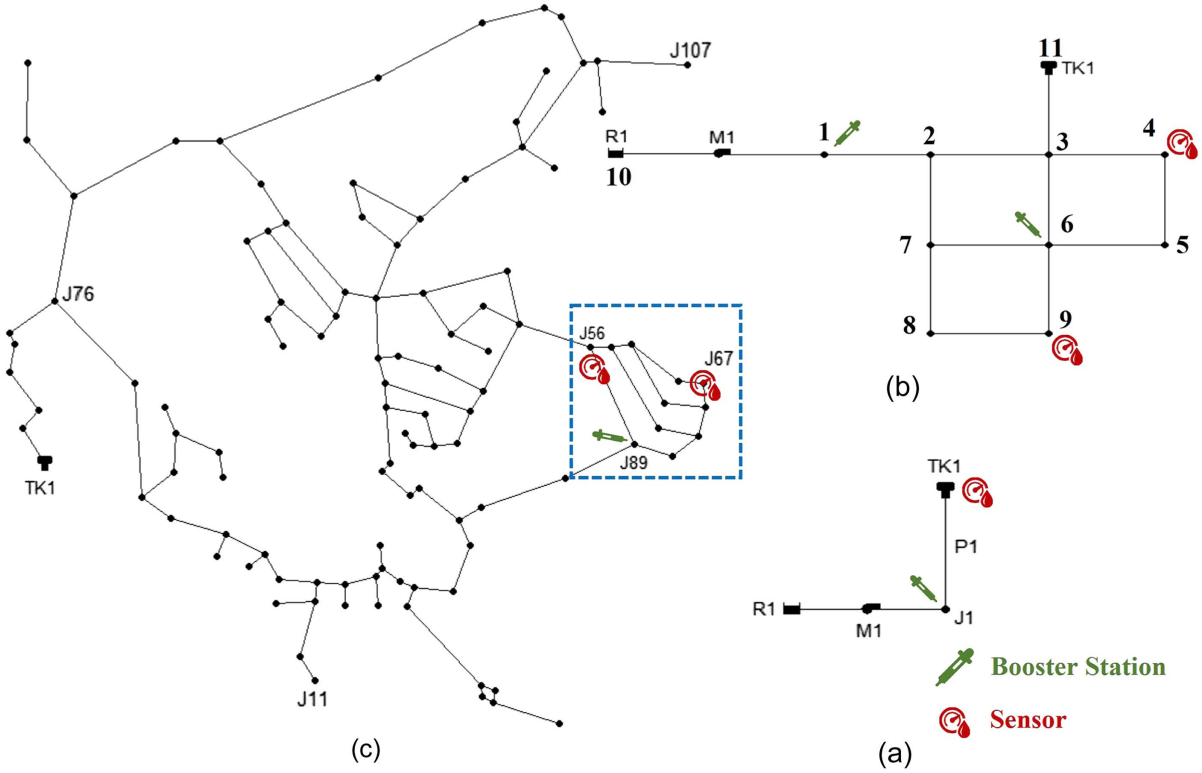

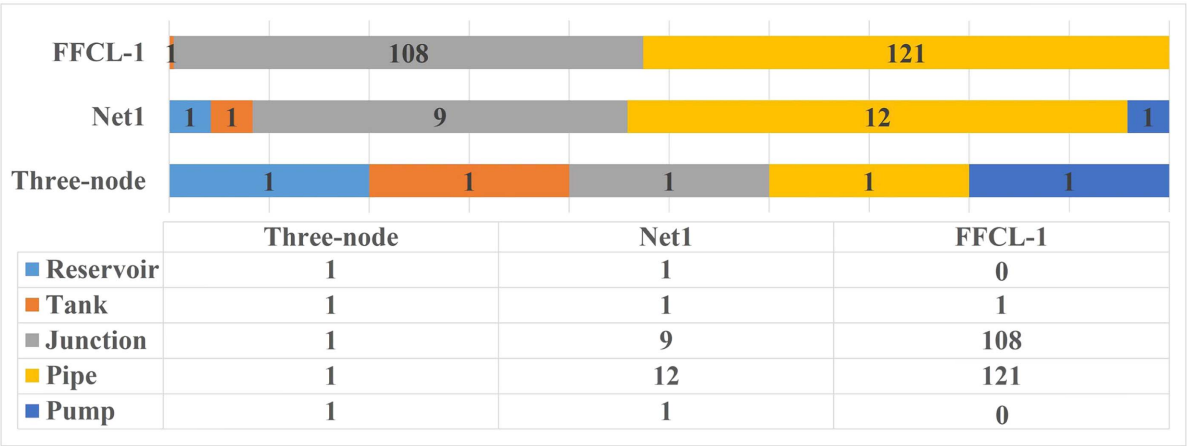

	Three-node	Net1	FFCL-1
Reservoir	1	1	0
Tank	1	1	1
Junction	1	9	108
Pipe	1	12	121
Pump	1	1	0

Fig. 6. Case studies' layouts and their components count: (a) three-node network; (b) Net1; and (c) FFCL-1 with the zone we control framed.

with different schemes for which fixing the operating point for all elements is not actively efficient. That is, we next investigate taking different operating points for each network component along the simulation window every specific number of time steps.

The choice of the operating points we linearize around is critical. The narrower the recurrent window of choosing the operating points, the closer the results to the original model. However, if we choose to update the operating points each water quality time step, then matrices $\breve{A}_{11}(t), \breve{A}_{12}(t), \breve{A}_{21}(t)$, and $\breve{A}_{22}(t)$ in Eq. (10) should be updated that frequently instead of being updated each hydraulic time step. It is acceptable for the hydraulic time step to be within an hourly scale to reflect the change in demand, while the range for water quality is between minutes and seconds to allow a stable numerical simulation (Shang et al. 2023; Seyoum and Tanyimboh 2017). Consequently, updating the aforementioned matrices every WQ time step adds more computational burden to the simulation, which negates the main reason for implementing linearization and model order reduction. On the contrary, widening the window to be more than the hydraulic time step especially in cases with significant demand change gives an inaccurate approximation of the system's behavior. Over and above that, it is important to consider falling within the control algorithm prediction and control horizon to be able to adjust accordingly with the controller input.

With the hydraulic setting of a patterned demand at J1 changing every 1 h [Fig. 8(c)], the model is linearized around operating points that are taken every 1 h for each of the network elements. The same sources of chemicals are provided at R1 with zero initial conditions for the other components. The results shown in Figs. 8(a and b) for chlorine concentrations at TK1 and P1 exhibit that updating operating points every 1 h results in accurate representation in comparison to the original model, except for the first hour, during which operating points are taken to be the initial concentrations at those elements. To mitigate this issue, operating points are updated after 1–10 min from the simulation start. The same approach

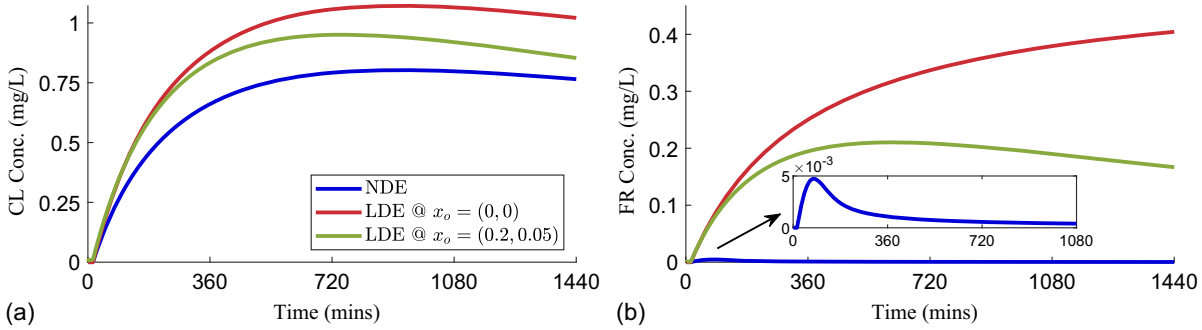

Fig. 7. Nonlinear versus linearized models results for (a) chlorine; and (b) fictitious reactant at TK1 of the three-node network.

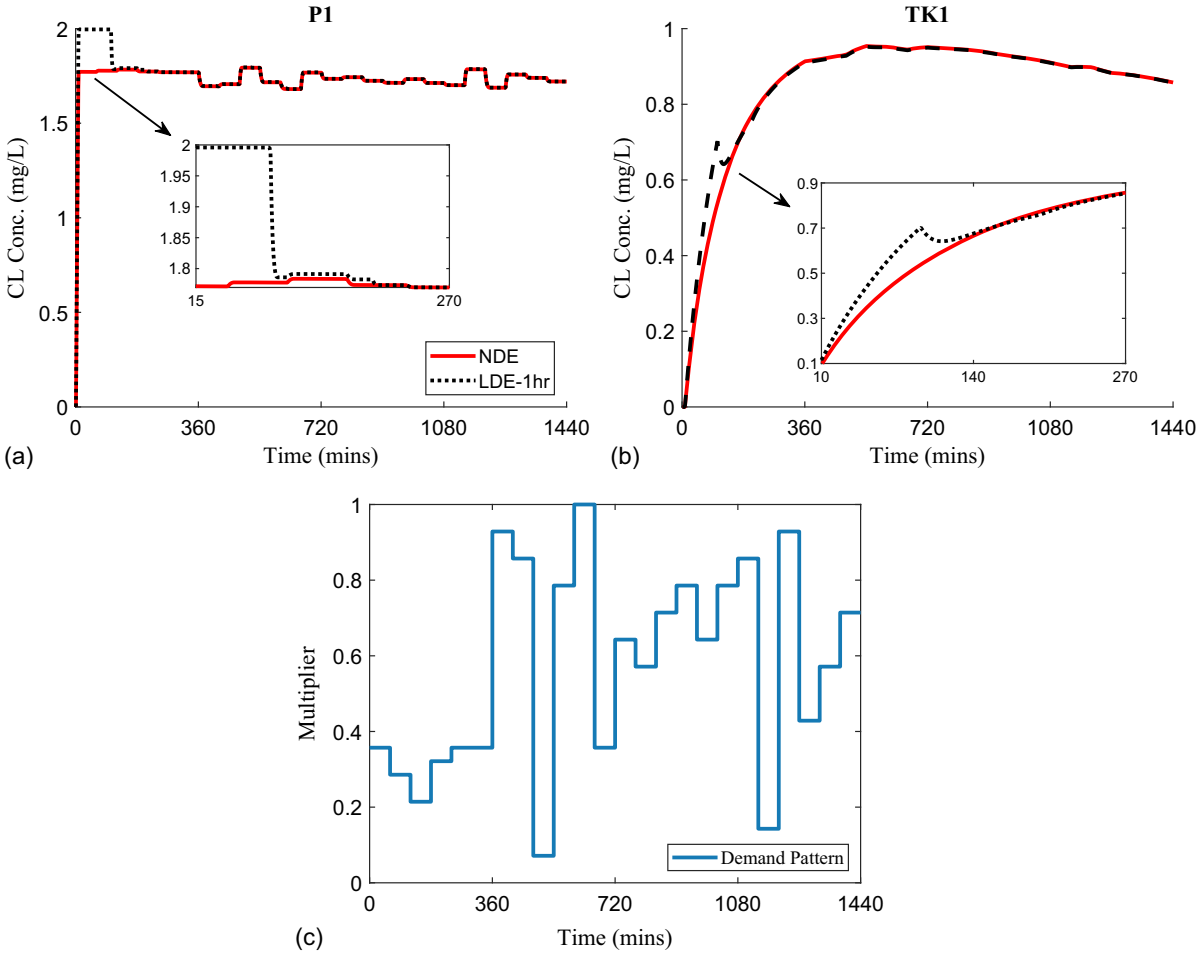

Fig. 8. Chlorine concentrations at (a) P1; and (b) TK1 of the three-node network; with (c) patterned demand at J1. Results are for the nonlinear and linearized models; linearization operating points are updated every hour for all network components.

is followed in scenarios where chemical dosages are increasing locally at some node for elements downstream of this node.

MS-WQ Model Order Reduction Performance

In this section, we assess and compare the performance of each of the proposed model order reduction procedures for multispecies water quality dynamics in terms of accuracy compared with the original full-order model and computational time. For each network, we apply POD and BPOD on the linearized model and extended POD for the nonlinear model. We refer to these procedures as LPOD, LBPOD, and NLPOD, respectively. We record the computational time needed for assembling the snapshots, obtaining the transformation matrices, and calculating the RMSE between the original and reduced-order model for a specific simulation under the same conditions.

First, we apply the three MOR methods on the three-node and Net1 networks under zero and nonzero initial conditions and static hydraulic profiles. The results shown in Figs. 9 and 10 validate that all methods are able to reduce the model dimensions with relatively

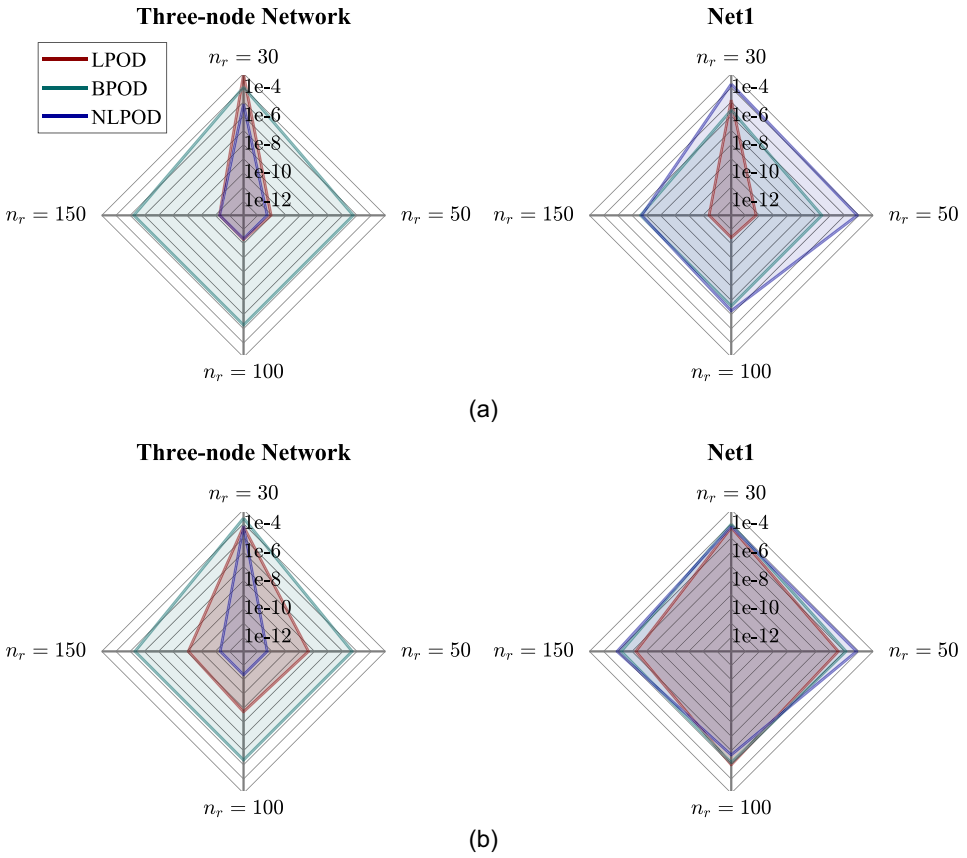

Fig. 9. RMSEs for the three proposed MOR methods for the three-node ($n_x = 204$) and Net1 ($n_x = 482$) networks with (a) zero; and (b) nonzero initial conditions for different n_r values.

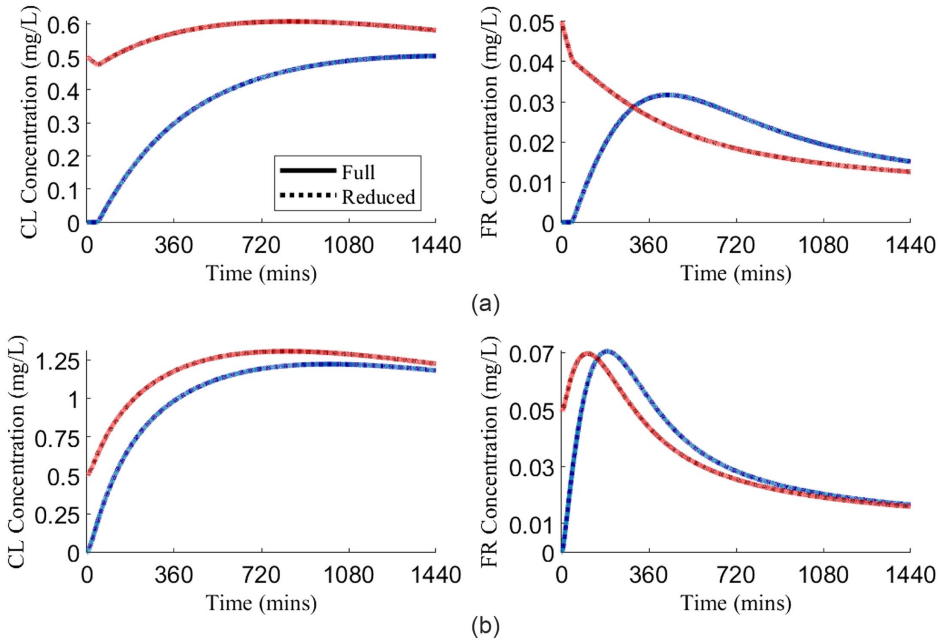

Fig. 10. Chlorine and fictitious reactant concentrations evolution at (a) TK1 of three-node network ($n_x = 204$); and (b) Tank 11 of Net1 ($n_x = 482$) under zero (in blue) and nonzero (in red) initial conditions simulated by full- and reduced-order models with $n_r = 30$ for both networks.

low RMSEs for different n_r values. These RMSEs get lower with increasing n_r values and are lower for the scenario of zero initial conditions compared with the case of nonzero initial conditions. For the scenario with nonzero initial conditions, initial chlorine concentrations are 0.5 mg/L network-wide; the initial fictitious reactant concentrations at TK1 in the three-node network and Tank 11 in Net1 are 0.05 mg/L. Fig. 10 shows the chlorine and fictitious reactant concentrations for both scenarios of initial conditions at

TK1 of the three-node network and Tank 11 of Net1 for the full-order model and the reduced-order models using all three MOR producers. The reduced-order models give almost identical results to the full-order one for the step response at TK1 and for a regular node along the network for Tank 1 for the two scenarios of zero and nonzero initial conditions. These results differ from Wang et al. (2022), where the POD method was found to have higher errors for the scenario of nonzero initial concentrations under single-species dynamics because the input-output relationship is not correctly captured when the initial values are treated as inputs into the system. In our study, this effect is mitigated by building the offline snapshot with a higher impulse signal by the booster stations, which results in favoring the actual locations of booster stations.

Meanwhile, MOR methods' performance is significantly impacted by the locations of the sensors and actuators and their reflection on network-wide observability and controllability. This leads to inaccurate or unstable results in some cases and in some other scenarios. However, the allocation of these sensors and actuators for each network is out of this paper's scope and we solve assuming the predetermination of their locations.

Model Order Reduction Sensitivity to System Hydraulics

The construction of the transformation matrices V_r and L_r for both methods POD and BPOD is sensitive to the snapshots (i.e., $\boldsymbol{X}_m$ and $\boldsymbol{P}_m$) constructed offline. These snapshots need to be long enough and representative of the actual reaction between states, inputs, and outputs. That leads to being sensitive to the hydraulic settings of the system while capturing these snapshots and also while applying the desired model reduction. Dynamic hydraulic states in a network reflect the consumers' patterned consumption, which can be recorded for a specific network during a specific season (Mazzoni et al. 2023).

After validating the reliability of the three MOR methods under zero and nonzero initial conditions, we investigate the case of dynamic hydraulic demands for a bigger network: the FFCL-1 network. In Fig. 11, the evolution of chlorine and the fictitious reactant at J11, J56, J76, and J107 of the FFCL-1 network simulated by the full-order model and LPOD-based reduced-order model is presented. Only LPOD is shown, which is representative of the behavior of all other approaches. In this scenario, an input of 0.3 mg/L for the fictitious reactant is inserted at the start of the network (i.e., at the tank) depicting an early intrusion event. As demonstrated, the LPOD-based ROM is able to trace the concentrations of the chemicals at different junctions, including dead-ends and junctions that connect looped pipes. Nonetheless, an oscillatory effect is detected for the fictitious reactant concentrations in the framed zone. This oscillation is formulated as the fictitious reactant being completely consumed by the chlorine at these junctions or at pipes flowing into them (e.g., J76). However, the operating points around which the system is linearized force the fictitious reactant to have false concentrations. Therefore, this effect is illuminated by applying NLPOD and is reduced by updating the operating points more frequently.

Last, the computational time recorded for each of the MOR method implementations on the three tested networks is illustrated in Fig. 12. For all networks, the NLPOD method requires more computational time as a result of handling the nonlinearity term separately and performing the greedy sampling algorithm. However, the maximum increase in time is around 95 s compared with BPOD for the FFCL-1 network, which is considered an acceptable computational time for a network of $n_x = 10{,}356$ states.

Implicit versus Explicit Discretization Schemes under Control–Theoretic Perspective

As stated in "Transport and Reaction in Pipes," the 1D AR equation can be discretized by implementing either explicit or implicit upwind schemes. The explicit scheme needs to be performed under a satisfied CFL condition to ensure stability, which requires a small time step in many cases and hence a higher system dimension. The implicit scheme is unconditionally stable but requires more complicated mathematical calculations that add to the computational work. Therefore, the following has been a pressing question: *Which is better: implicit or explicit discretization schemes?* This has proven to not have an easy answer. In our study, we reduce our system's dimensions while applying either of these methods. Nonetheless, while transformation matrices are calculated offline, some system matrices are updated every hydraulic time step. This adds more computational load with matrices multiplication, which is higher with the matrix inverse in the case of the implicit scheme. Also, although the implicit scheme allows a larger simulation time step, a smaller one is more efficient to be able to update the control inputs more frequently. So our question can be formulated as follows: *From a control–theoretic perspective, which is better: implicit or explicit discretization schemes?*

Because model order reduction is a prior step to applying control to our model, we test both discretization methods' performance while applying the LPOD method for Net1. As demonstrated in Fig. 13(a), the RMSEs are lower for the implicit than the explicit scheme. In addition, the change in RMSEs by increasing n_r more

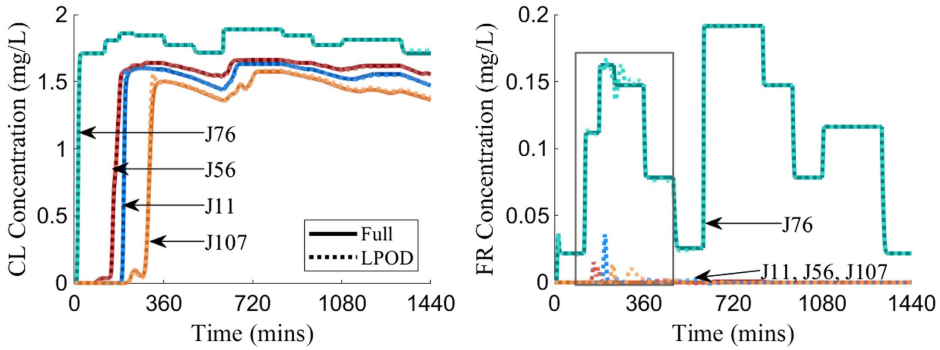

Fig. 11. Chlorine and fictitious reactant concentrations evolution at J11, J56, J76, and J107 of the FFCL-1 network simulated by full- and reduced-order models. Full-order model results for at each of the junctions are in solid lines, while the LPOD method results are in dashed lines. The number of states for the full-order model is $n_x = 10{,}356$ and reduced to $n_r = 200$ states.

J. Water Resour. Plann. Manage., 2024, 150(2): 04023077

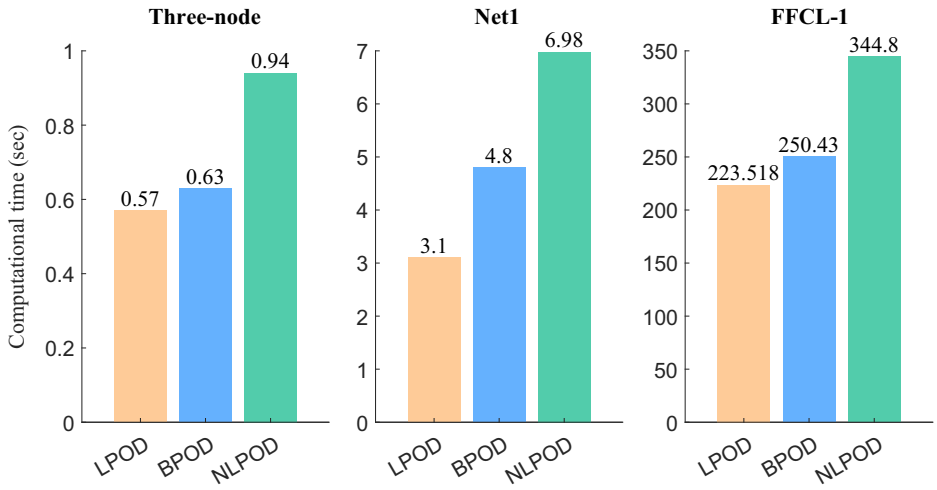

Fig. 12. Computational time to implement the three MOR methods for three tested networks. Total number of states n_x is 10,356 for FFCL-1, 482 for Net1, and 204 for the three-node network.

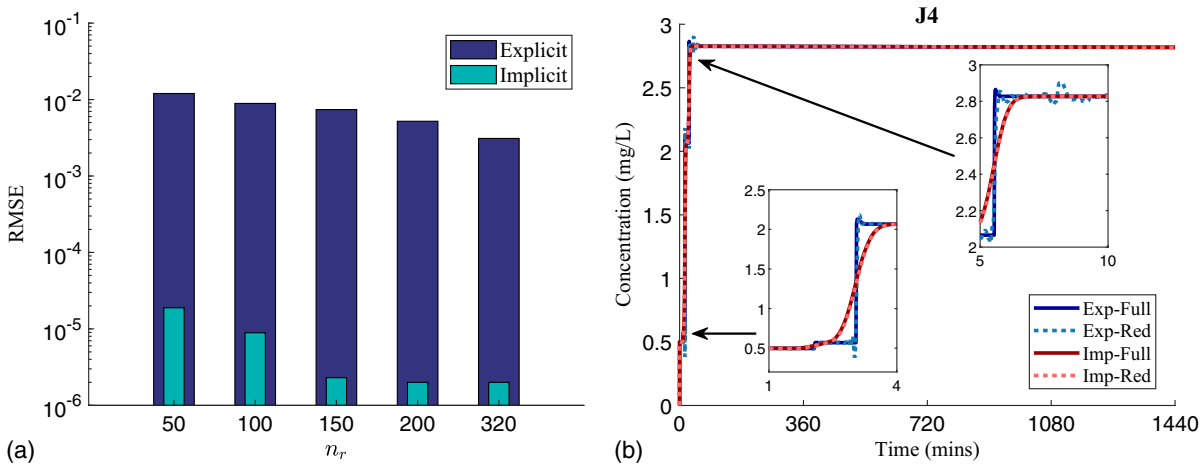

Fig. 13. (a) RMSEs for the reduced-order explicit and implicit upwind schemes–based models while applying LPOD on Net1 with $n_x = 482$ for different n_r values; and (b) chlorine concentrations at J4 simulated by the full- and reduced-order models (with $n_r = 100$) using both schemes.

than 150 is insignificant because the states that get retained do not hold high energy compared to the previously selected ones. On the other hand, the error values for the explicit scheme do not go lower than 0.003 with increasing n_r—explained through the following example. Although the CFL condition is satisfied for the explicit scheme, it formulates sharp fronts at points with a relatively significant change in the chemical concentrations as shown in Fig. 13(b). Fig. 13(b) illustrates chlorine concentrations at J4 for both implicit and explicit schemes and the corresponding reduced models with $n_r = 120$ of a full model with $n_x = 482$. It is noticeable that the reduced model, based on the explicit scheme, exhibits instability behavior initially, but this behavior gradually dampens, allowing the system to eventually reach equilibrium. This performance is recorded under a low Courant number with the network's pipes. To mitigate that, the water quality time step is required to be reduced to reach a higher CN—near but less than 1. Such behavior is avoided when applying the unconditionally stable implicit scheme.

To that end, the implicit upwind scheme gives more accurate results that lead to a more robust control algorithm. The computational burden of this scheme can be lowered using sparse matrix multiplication. The computational times to perform the simulation on Net1 shown in Fig. 13(a) are 32.9 and 43.4 s for the explicit and implicit upwind schemes, respectively, for the same water quality time step. However, the implicit scheme retains high accuracy under a higher WQ time step while requiring lower computational run time. Therefore, the implicit upwind scheme gives more flexibility in choosing the time step needed to retain real-time control windows while maintaining high accuracy.

Real-Time Control Implementation of MS-WQM MOR-Based MPC

The main objective of this paper and the prior investigation of the MOR methods is to integrate them into and apply a real-time control algorithm of chlorine concentrations using the booster stations distributed along the WDN under MS-WQM. We apply the MPC algorithm on the linearized and nonlinearized MS-WQ ROM as explained in "Real-Time Regulation of MS-WQM via Model Predictive Control and McCormick Relaxations." Because both LPOD and BPOD can reduce the MS-WQM effectively, for the linearized

model we apply the BPOD method. On the other hand, we apply NLPOD for the nonlinear model to obtain the ROM.

For multispecies water quality control and regulation, while applying the McCormick relaxation, the envelopes rely on the limits for both chemicals. For the network's components near the location of the second chemical intrusion, these envelopes put tight boundaries on the chosen value for z by the control problem because x_2 is close to $x_2^{\max}$. On the other hand, for components downstream from this location with lower concentrations for both chemicals, the relaxation allows higher and lower values for z, which leads to choosing a value of z to be as close to the underestimators so the control inputs are lower and the cost of chlorine injections is reduced. Additionally, for higher values of the mutual reaction coefficient k_r, the effect of relaxation on the chosen control input increases. That is, the proposed relaxed MPC may result in overlooking or underestimating the mutual reaction and, therefore, we lowered the upper bound for the fictitious reactant as a procedure integrated into the looped control algorithm repeated each time step.

As explained in "Nonlinear versus Linearized Models," it is proposed to update the operating points around which the system is linearized every significant change window (e.g., hydraulic states change). Updating these operating points adds to the computational time by recalculating the matrices, yet it yields a more accurate representation. Therefore, we put a threshold according to which we judge changing these points after applying every control input.

By adopting these approaches, we start with applying the MS-WQC-MPC-based method on the three-node network under a static hydraulic profile and with a reduced number of states of $n_r = 30$ out of $n_x = 204$. The water quality time step is chosen to be 5 s and the control horizon is 10 min. The fictitious reactant was discharged into the system at J1 (same location of the booster station) at a concentration of 0.1 mg/L for the first hour of the simulation. Fig. 14 demonstrates the control actions and the corresponding control response in J1 and P1 under the multispecies linearized ROM, nonlinear ROM, and single-species ROM that neglects the existence of the other chemical in the system for the first consecutive 2 h of simulation. For all scenarios, chlorine concentrations at J1 and P1 are zero at the start of the simulation. That is, MPC starts by injecting high chlorine dosage of 21,284 mg/min for the case of multispecies dynamics and 20,838 mg/min for the single-species model. The control input needed drops to 19,158 and 17,596 mg/min for multispecies and single-species dynamics, respectively. After the first hour of simulation, MPC results in the same control actions for both models as the intrusion event is contained. The second substance's initial concentration for P1 is zero, which leads to the peak control action at the start of the simulation being relatively close because the second substance has not traveled into P1. Comprehensively, this highlights the importance and effectiveness of the adopted MS-WQM and control framework. Furthermore, this difference between the two models' results (i.e., chlorine concentration dynamics and optimal chlorine inputs) increases for more reactive components with chlorine and initial intrusion concentrations, which may cause operational issues with limited chlorine availability and/or budget.

Additionally, the linearized MS-WQC problem and relaxed one produce the same performance as illustrated in Fig. 14(a). In the linearized model, the operating points are updated at the beginning of the simulation, following the application of the peak control action, and once again at the end of the contamination event. For the relaxed MS-WQC problem, all elements are directly affected by the event, resulting in tight envelopes and approximating the mutual reaction near its actual value. However, the number of control variables for this procedure is higher for the first hour. To that end, the computational time needed for each of the two control procedures is case oriented. For this case study, the linearized-based MPC method has computational time of 78 s, while it is 93 s for the second method.

Next, we apply the proposed MS-WQC approach on Net1 under a dynamic hydraulic profile defined by the patterned demand at Junction 1 [Fig. 15(c)]. The FOM has 482 states, which are reduced to 50. Because both control procedures have proved their ability to regulate chlorine concentrations network-wide, we showcase the results from the relaxed MPC procedure only to point out case studies that can take place. In this case study, the water quality time step is 5 s, while the control horizon is 10 min and the simulation period is 24 h. The initial concentrations of all chemicals are zero. The fictitious reactant is set to intrude the system at Junction 6 with a concentration of 0.3 mg/L mid-day. Additionally, chlorine concentrations are limited to 1.2 mg/L for cost reasons. For this case study, we introduce two types of disturbance to the system: a sudden drop in chlorine concentration at Junction 6 to 0.15 mg/L at the 12th hour of the day and a sudden increase to 2 mg/L at the 18th hour. Fig. 15(a) shows the control action at Junctions 1 and 6, while Fig. 15(b) demonstrates the corresponding chlorine concentrations at these junctions and Junctions 5 and 8. For Junction 1, the control action is higher and almost constant at 1.9×10^4 mg/min because the junction is located at the very start of the network and all the downstream elements are affected by its input. On the other hand, the booster station at Junction 6 acts on the disturbances and the changes at the downstream nodes effectively. The results validate the performance of the control algorithm and how adaptive it is under these disturbances. The run time recorded for applying the

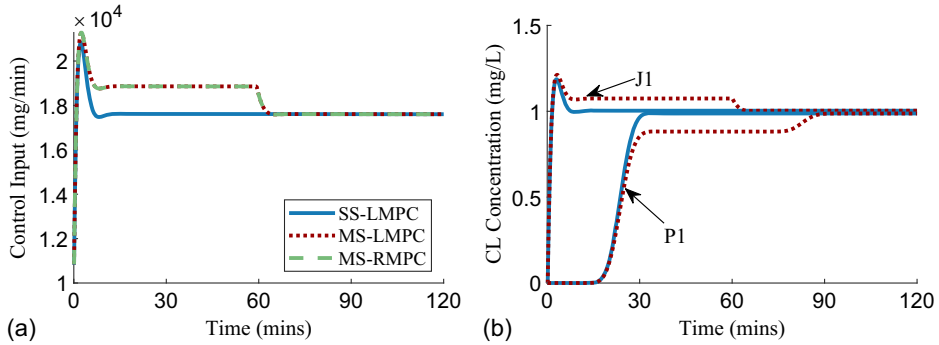

Fig. 14. (a) Control action $\mathbf{u}_1$ during 2 h of simulation on the three-node network by applying SS-LMPC: linear single-species-based MPC, MS-LMPC: linearized multispecies-based MPC, and MS-RMPC: nonlinear multispecies-based relaxed MPC; and (b) chlorine concentrations at J1 and P1 under another chemical intrusion at J1 for the first hour.

J. Water Resour. Plann. Manage., 2024, 150(2): 04023077

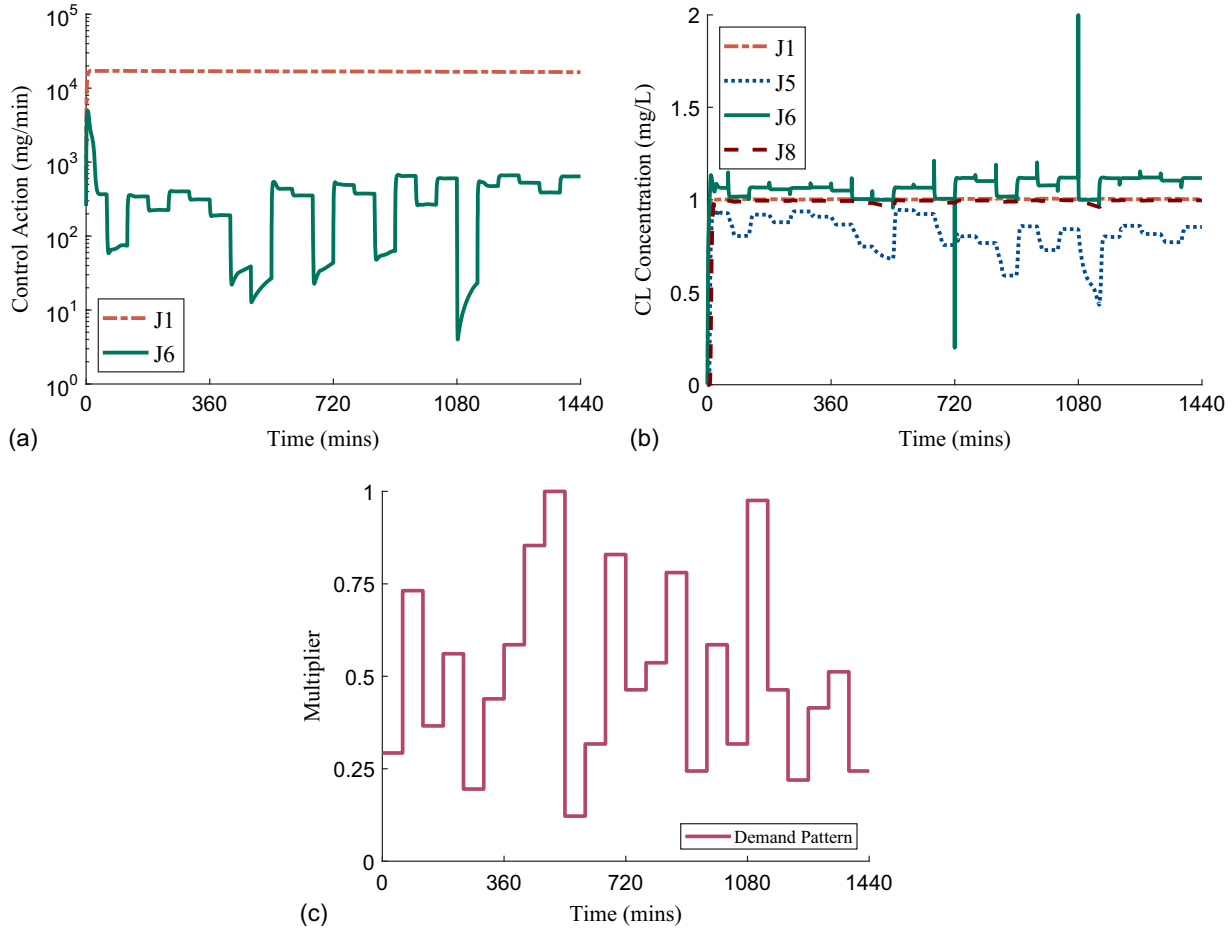

Fig. 15. (a) MPC control action at Junctions 1 and 6 of Net1; (b) the corresponding chlorine concentrations at these junctions and Junctions 5 and 8 under; and (c) patterned demand at Junction 1.

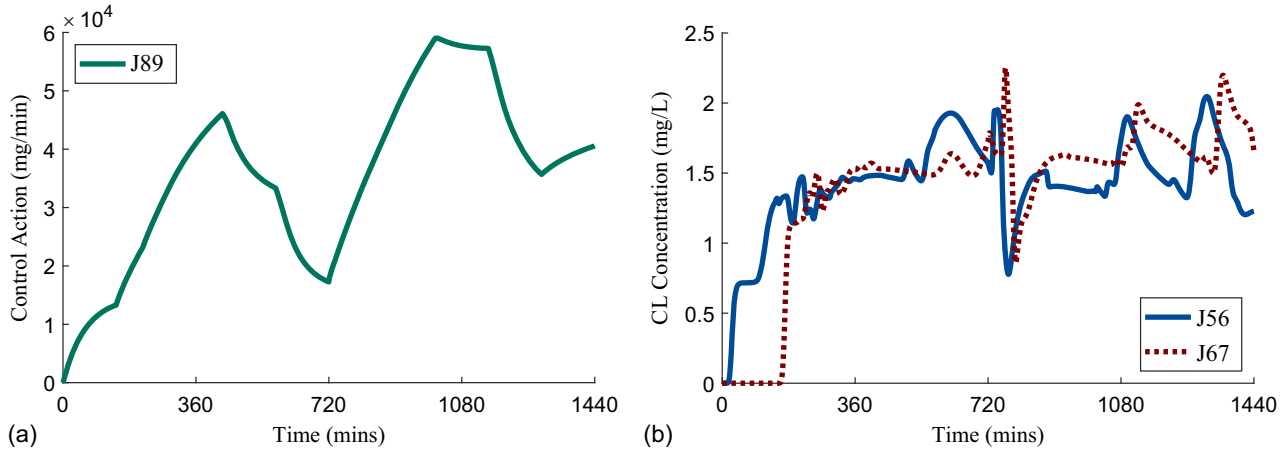

Fig. 16. (a) Control action at J89 of the FFCL-1 network; and (b) the corresponding chlorine concentrations at J56 and J67.

control algorithm for this case study is 278 s. Likewise, chlorine concentrations are regulated through the FFCL-1 network as Fig. 16 exhibits. The total number of states of the original model is 10,356, while the reduced model has 200 states. Water quality time step, control horizon, and simulation period are the same as the previous case study. Two different fictitious reactants are assumed to be detected, the first one at J76 with initial concentration of 0.3 mg/L and the second one at J89 with 0.2 mg/L. Control actions illustrated in Fig. 16(a) are under the condition of hydraulic profile that results in changing flow directions. Yet, the control algorithm recovers effectively and maintains chlorine concentrations within the desired range. In short, the ROMs-based control algorithms guarantee the bounds defined for the inputs and outputs while being tractable for larger networks.

J. Water Resour. Plann. Manage., 2024, 150(2): 04023077

Conclusion, Paper's Limitations, and Recommendations for Future Work

Relying on the results from the numerical case studies in "Case Studies," we answer the research questions in the order they are posed:

1. The multispecies water quality model can be effectively linearized around operating points updated every specific moving window according to the hydraulic profile, instantaneous changes, initial conditions, and control actions. However, to achieve the desired accuracy, this window is reduced, and accordingly the computational time increases.
2. The presented MOR methods yield high accuracy in estimating output concentrations for both chlorine and the fictitious substance in the system. The three MOR procedures LPOD, BPOD, and NLPOD are able to handle nonzero initial conditions by favoring the control actuators' inputs while building the offline snapshots. Additionally, the NLPOD method requires more computational time to handle and interpolate the nonlinearity in the system, yet it is still computationally tractable; the same is true for LPOD and BPOD.
3. MPC's behavior depends on the underlying model and its accuracy. Accordingly, the implicit upwind scheme is preferred over the explicit upwind scheme because of its ability to provide highly accurate simulation for the full- and reduced-order MS-WQM. Moreover, numerical case studies show that the three MOR producers are robust to dynamically changing hydraulic profiles.
4. MPC shows robustness and high flexibility in regulating chlorine levels in WDNs under different scenarios of contamination events and hydraulic profiles by applying feedback control on the reduced-order model while maintaining affordable computational requirements. Both proposed control procedures, the linearized model and the relaxed nonlinear model based, show reliable performance while applying adaptive approaches according to the case study considered. These approaches lead to a different level of complexity and computational burden for each of the procedures, which results in favoring one procedure over the other according to the case study.

Our study is not limitations free. We highlight these limitations next along with our future work. First, this work use preassigned fixed-location booster and sensor locations. Given that these locations impact performance, future work will include optimizing them from a control–theoretic perspective. Second, additional approaches to model linearization should be explored to potentially exploit offline precomputed FOM trajectories. Last, further work is needed to improve the relaxation method because we expect opportunities to further improve computational performance compared to the linearized model. This study is considered a computational study that is based on a model that has been verified; however, a real-time experimental study to verify the considered model and our framework performance under various scenarios is recommended.

Data Availability Statement

All data, models, and codes that support the findings of this study are available from the corresponding author upon reasonable request.

Acknowledgments

This work is partially supported by National Science Foundation under Grants 1728629, 2015603, 2015671, 2151392, and 2015658.

References

Acrylamide, T. 2009. "National primary drinking water regulations." *Kidney* 2 (4-D): 1–7.

Akkari, N., F. Casenave, and D. Ryckelynck. 2019. *A novel gappy reduced order method to capture non-parameterized geometrical variation in fluid dynamics problems*. Bangalore, India: Hindustan Aeronautics Limited.

Antoulas, A. C., D. C. Sorensen, and S. Gugercin. 2000. *A survey of model reduction methods for large-scale systems*. Rep. No. 719. Houston: Rice Univ.

Apostol, T. M. 1991. Vol. 1 of *Calculus*. New York: Wiley.

Barrachina, S., P. Benner, E. S. Quintana-Ortí, and G. Quintana-Ortí. 2005. "Parallel algorithms for balanced truncation of large-scale unstable systems." In *Proc., 44th IEEE Conf. on Decision and Control*, 2248–2253. New York: IEEE.

Baur, U., P. Benner, and L. Feng. 2014. "Model order reduction for linear and nonlinear systems: A system-theoretic perspective." *Arch. Comput. Methods Eng.* 21 (4): 331–358. https://doi.org/10.1007/s11831-014-9111-2.

Beattie, C. A., and S. Gugercin. 2008. "Interpolation theory for structure-preserving model reduction." In *Proc., 47th IEEE Conf. on Decision and Control*, 4204–4208. New York: IEEE.

Benner, P., S. Gugercin, and K. Willcox. 2015. "A survey of projection-based model reduction methods for parametric dynamical systems." *SIAM Rev.* 57 (4): 483–531. https://doi.org/10.1137/130932715.

Carlberg, K., C. Farhat, J. Cortial, and D. Amsallem. 2013. "The GNAT method for nonlinear model reduction: Effective implementation and application to computational fluid dynamics and turbulent flows." *J. Comput. Phys.* 242 (Mar): 623–647. https://doi.org/10.1016/j.jcp.2013.02.028.

Chen, Y. 1999. "Model order reduction for nonlinear systems." Ph.D. thesis, Dept. of Mathematics, Massachusetts Institute of Technology.

Diao, K., and W. Rauch. 2013. "Controllability analysis as a pre-selection method for sensor placement in water distribution systems." *Water Res.* 47 (16): 6097–6108. https://doi.org/10.1016/j.watres.2013.07.026.

Elkhashap, A., and D. Abel. 2022. "Model order reduction of the time-dependent advection-diffusion-reaction equation with time-varying coefficients: Application to real-time water quality monitoring." In *Proc., 2022 European Control Conf. (ECC)*, 333–338. New York: IEEE.

Elsherif, S. M., S. Wang, A. F. Taha, L. Sela, M. H. Giacomoni, and A. A. Abokifa. 2022. "Control-theoretic modeling of multi-species water quality dynamics in drinking water networks: Survey, methods, and test cases." *Annu. Rev. Control* 55 (Jun): 466–485. https://doi.org/10.1016/j.arcontrol.2022.08.003.

Fisher, I., G. Kastl, F. Shang, and A. Sathasivan. 2018. "Framework for optimizing chlorine and byproduct concentrations in drinking water distribution systems." *J. Am. Water Works Assoc.* 110 (11): 38–49. https://doi.org/10.1002/awwa.1183.

Fu, B., et al. 2020. "Modeling water quality in watersheds: From here to the next generation." *Water Resour. Res.* 56 (11): e2020WR027721. https://doi.org/10.1029/2020WR027721.

Galbally, D., K. Fidkowski, K. Willcox, and O. Ghattas. 2010. "Non-linear model reduction for uncertainty quantification in large-scale inverse problems." *Int. J. Numer. Methods Eng.* 81 (12): 1581–1608. https://doi.org/10.1002/nme.2746.

Grimme, E. J. 1997. *Krylov projection methods for model reduction*. Champaign, IL: Univ. of Illinois at Urbana-Champaign.

Gugercin, S. 2008. "An iterative SVD-Krylov based method for model reduction of large-scale dynamical systems." *Linear Algebra Appl.* 428 (8–9): 1964–1986. https://doi.org/10.1016/j.laa.2007.10.041.

He, J., and L. J. Durlofsky. 2014. "Reduced-order modeling for compositional simulation by use of trajectory piecewise linearization." *SPE J.* 19 (5): 858–872. https://doi.org/10.2118/163634-PA.

Hirsch, C. 1990. "Numerical computation of internal and external flows." Vol. 2 of *Computational methods for inviscid and viscous flows*. Chichester, UK: Wiley.

Kumar, R., and D. Ezhilarasi. 2022. "A state-of-the-art survey of model order reduction techniques for large-scale coupled dynamical systems."

Int. J. Dyn. Control 11 (2): 900–916. https://doi.org/10.1007/s40435-022-00985-7.

Lall, S., J. E. Marsden, and S. Glavaški. 1999. "Empirical model reduction of controlled nonlinear systems." *IFAC Proc. Volumes* 32 (2): 2598–2603. https://doi.org/10.1016/S1474-6670(17)56442-3.

Lall, S., J. E. Marsden, and S. Glavaški. 2002. "A subspace approach to balanced truncation for model reduction of nonlinear control systems." *Int. J. Robust Nonlinear Control: IFAC-Affiliated J.* 12 (6): 519–535. https://doi.org/10.1002/rnc.657.

Lassila, T., A. Manzoni, A. Quarteroni, and G. Rozza. 2014. "Model order reduction in fluid dynamics: Challenges and perspectives." In *Reduced order methods for modeling and computational reduction*, edited by A. Quarteroni and G. Rozza, 235–273. Cham, Switzerland: Springer International.

Li, Z., S. G. Buchberger, and V. Tzatchkov. 2005. "Importance of dispersion in network water quality modeling." In *Impacts of global climate change*, 1–12. Reston, VA: ASCE. https://doi.org/10.1061/40792(173)27.

Liu, Y.-Y., and A.-L. Barabási. 2016. "Control principles of complex systems." *Rev. Mod. Phys.* 88 (3): 035006. https://doi.org/10.1103/RevModPhys.88.035006.

Luchtenburg, D. M., and C. W. Rowley. 2011. "Model reduction using snapshot-based realizations." *Bull. Am. Phys. Soc.* 56 (18).

Martnez Alzamora, F., B. Ulanicki, and E. Salomons. 2014. "Fast and practical method for model reduction of large-scale water-distribution networks." *J. Water Resour. Plann. Manage.* 140 (4): 444–456. https://doi.org/10.1061/(ASCE)WR.1943-5452.0000333.

Mazzoni, F., et al. 2023. "Investigating the characteristics of residential end uses of water: A worldwide review." *Water Res.* 230 (Feb): 119500. https://doi.org/10.1016/j.watres.2022.119500.

McCormick, G. P. 1976. "Computability of global solutions to factorable nonconvex programs: Part I—Convex underestimating problems." *Math. Program.* 10 (1): 147–175. https://doi.org/10.1007/BF01580665.

Montier, L., T. Henneron, B. Goursaud, and S. Clenet. 2017. "Balanced proper orthogonal decomposition applied to magnetoquasi-static problems through a stabilization methodology." *IEEE Trans. Magnage.* 53 (7): 1–10. https://doi.org/10.1109/TMAG.2017.2683448.

Moore, B. 1981. "Principal component analysis in linear systems: Controllability, observability, and model reduction." *IEEE Trans. Autom. Control* 26 (1): 17–32. https://doi.org/10.1109/TAC.1981.1102568.

Munavalli, G. R., and M. S. M. Kumar. 2003. "Optimal scheduling of multiple chlorine sources in water distribution systems." *J. Water Resour. Plann. Manage.* 129 (6): 493–504. https://doi.org/10.1061/(ASCE)0733-9496(2003)129:6(493).

Nguyen, V. B., S. B. Q. Tran, S. A. Khan, J. Rong, and J. Lou. 2020. "POD-DEIM model order reduction technique for model predictive control in continuous chemical processing." *Comput. Chem. Eng.* 133 (May): 106638. https://doi.org/10.1016/j.compchemeng.2019.106638.

Ohar, Z., and A. Ostfeld. 2014. "Optimal design and operation of booster chlorination stations layout in water distribution systems." *Water Res.* 58 (Aug): 209–220. https://doi.org/10.1016/j.watres.2014.03.070.

Ostfeld, A., and E. Salomons. 2006. "Conjunctive optimal scheduling of pumping and booster chlorine injections in water distribution systems." *Eng. Optim.* 38 (3): 337–352. https://doi.org/10.1080/03052150500478007.

Palansooriya, K. N., Y. Yang, Y. F. Tsang, B. Sarkar, D. Hou, X. Cao, E. Meers, J. Rinklebe, K.-H. Kim, and Y. S. Ok. 2020. "Occurrence of contaminants in drinking water sources and the potential of biochar for water quality improvement: A review." *Crit. Rev. Environ. Sci. Technol.* 50 (6): 549–611. https://doi.org/10.1080/10643389.2019.1629803.

Perelman, L., and A. Ostfeld. 2008. "Water distribution system aggregation for water quality analysis." *J. Water Resour. Plann. Manage.* 134 (3): 303–309. https://doi.org/10.1061/(ASCE)0733-9496(2008)134:3(303).

Preis, A., A. J. Whittle, A. Ostfeld, and L. Perelman. 2011. "Efficient hydraulic state estimation technique using reduced models of urban water networks." *J. Water Resour. Plann. Manage.* 137 (4): 343–351. https://doi.org/10.1061/(ASCE)WR.1943-5452.0000113.

Rossman, L., H. Woo, M. Tryby, F. Shang, R. Janke, and T. Haxton. 2020. *EPANET 2.2 user manual water infrastructure division, center for environmental solutions and emergency response*. Cincinnati: USEPA.

Rowley, C. W. 2005. *Model reduction for fluids, using balanced proper orthogonal decomposition*, 17. Singapore: World Scientific.

Rutzmoser, J. 2018. "Model order reduction for nonlinear structural dynamics." Ph.D. thesis, Technische Universität München.

Schilders, W. H. A., et al., eds. 2008. "Model order reduction: Theory, research aspects and applications." In Vol. 13 of *Mathematics in industry.* Berlin: Springer.

Seyoum, A. G., and T. T. Tanyimboh. 2017. "Integration of hydraulic and water quality modelling in distribution networks: EPANET-PMX." *Water Resour. Manage.* 31 (14): 4485–4503. https://doi.org/10.1007/s11269-017-1760-0.

Shamir, U., and E. Salomons. 2008. "Optimal real-time operation of urban water distribution systems using reduced models." *J. Water Resour. Plann. Manage.* 134 (2): 181–185. https://doi.org/10.1061/(ASCE)0733-9496(2008)134:2(181).

Shang, F., L. A. Rossman, and J. G. Uber. 2023. *EPANET-MSX 2.0 user manual*. EPA/600/R-22/199. Cincinnati: USEPA.

Shang, F., H. Woo, J. B. Burkhardt, and R. Murray. 2021. "Lagrangian method to model advection-dispersion-reaction transport in drinking water pipe networks." *J. Water Resour. Plann. Manage.* 147 (9): 04021057. https://doi.org/10.1061/(ASCE)WR.1943-5452.0001421.

Sirovich, L. 1987. "Turbulence and the dynamics of coherent structures. I. Coherent structures." *Q. Appl. Math.* 45 (3): 561–571. https://doi.org/10.1090/qam/910462.

Ulanicki, B., A. Zehnpfund, and F. Martinez. 1996. "Simplification of water distribution network models." In *Proc., 2nd Int. Conf. on Hydroinformatics*, 493–500. Rotterdam, Netherlands: A. A. Balkema.

Wang, S., A. Chakrabarty, and A. F. Taha. 2023. "Data-driven identification of dynamic quality models in drinking water networks." *J. Water Resour. Plann. Manage.* 149 (4): 04023008. https://doi.org/10.1061/JWRMD5.WRENG-5431.

Wang, S., A. F. Taha, and A. A. Abokifa. 2021. "How effective is model predictive control in real-time water quality regulation? State-space modeling and scalable control." *Water Resour. Res.* 57 (5): e2020WR027771. https://doi.org/10.1029/2020WR027771.

Wang, S., A. F. Taha, A. Chakrabarty, L. Sela, and A. A. Abokifa. 2022. "Model order reduction for water quality dynamics." *Water Resour. Res.* 58 (4): e2021WR029856. https://doi.org/10.1029/2021WR029856.

Willcox, K., and J. Peraire. 2002. "Balanced model reduction via the proper orthogonal decomposition." *AIAA J.* 40 (11): 2323–2330. https://doi.org/10.2514/2.1570.

Yang, Y. J., R. C. Haught, and J. A. Goodrich. 2009. "Real-time contaminant detection and classification in a drinking water pipe using conventional water quality sensors: Techniques and experimental results." *J. Environ. Manage.* 90 (8): 2494–2506. https://doi.org/10.1016/j.jenvman.2009.01.021.

Zhou, K., G. Salomon, and E. Wu. 1999. "Balanced realization and model reduction for unstable systems." *Int. J. Robust Nonlinear Control: IFAC-Affiliated J.* 9 (3): 183–198. https://doi.org/10.1002/(SICI)1099-1239(199903)9:3<183::AID-RNC399>3.0.CO;2-E.